< Electronic Supporting Information>

Combination of Aluminum Molecular Rings with Chemical Reduction Centers for Iodine Capture and Aggregation

Dan Luo, Fei Wang, Chen-Hui Liu, San-Tai Wang, Ya-Yong Sun, Wei-Hui Fang* and Jian Zhang

State Key Laboratory of Structural Chemistry, Fujian Institute of Research on the Structure of Matter, Chinese Academy of Sciences, Fuzhou, Fujian 350002, China
Email: fwh@fjirsm.ac.cn.

Content

1. Synthesis

Synthesis of AlOC-150

A mixture of aluminum isopropoxide (204 mg, 1 mmol), 3-Aminoisonicotinic acid (210 mg, 1.52 mmol); Iron (III) chloride anhydrous (60 mg, 0.37 mmol), methylamine ethanol solution (40 %, 120 μL), n-butanol (2.5 mL) and DMF (2.5 mL) was sealed in a 20 mL vial and transferred to a preheated oven at 120 °C for 4 days. When cooled to room temperature, orange crystals were obtained. (yield: 65 % based on $Al(O^iPr)_3$). The crystals are rinsed with DMF and preserved under a sealed and dry environment. FT-IR (KBr, cm^{-1}): 3453(s), 3074(w), 2958(w), 2850(w), 2706(m), 1661(s), 1597(m), 1490(s), 1252(m), 1047(m), 995(m), 910(s), 754(s) 702(m), 682(m), 630(m), 511(s). Elemental analysis calcd. (%) for $Al_8Fe_2Cl_4C_{104}N_{24}O_{43}H_{142}$ (MW 2885.75): C 43.25, N 11.65, H 4.96; found C 45.46, N 13.58, H 5.75.

Synthesis of AlOC-151 - AlOC-154

A mixture of aluminum isopropoxide (204 mg, 1 mmol), isonicotinic acid (120 mg, 1 mmol), Iron (III) chloride anhydrous or Chromium (II) chloride hexahydrate or Nickel (II) chloride hexahydrate or Iron (III) bromide anhydrous (60 mg, 0.37 mmol; 30 mg, 0.13 mmol; 30 mg, 0.25mmol; 90 mg, 0.3 mmol), methylamine ethanol solution (40 %, 120 μL), n-butanol (2.5 mL) and DMF (2.5 mL) was sealed in a 20 mL vial and transferred to a preheated oven at 100 °C for 4 days. When cooled to room temperature, deep red **AlOC-151**, light pink **AlOC-152**, light green **AlOC-153** and red crystals **AlOC-154** were obtained. The crystals are rinsed with DMF and preserved under a sealed and dry environment. (yield: 53 %; 25 %; 28 %; 36% based on $Al(O^iPr)_3$). **AlOC-151**-FT-IR (KBr, cm^{-1}): 2954(w), 2917(w), 2868(w), 2842(w), 1674(m), 1607(s), 1552(s), 1491(s), 1443(s), 1215(w), 1127(w), 1063(m), 997(w) 782(m), 694(m), 562(m). **AlOC-152**-FT-IR (KBr, cm^{-1}): 3389(w), 3217(w), 2961(w), 2868(w), 1610(s), 1545(s), 1500(m), 1444(s), 1374(s), 1225(w), 1056(m), 1013(w), 858(w) 777(m), 701(m), 557(m). **AlOC-153**-FT-IR (KBr, cm^{-1}): 3444(s), 2969(w), 1614(s), 1545(s), 1437(w), 1397(w), 1342(w), 1232(w), 1163(w), 1067(w), 873(w), 768(m), 722(w) 693(w). **AlOC-154**-FT-IR (KBr, cm^{-1}): 3401(s), 2961(m), 2874(w), 1608(s),1542(s), 1501(m), 1449(s), 1223(w), 1064(m), 780(m), 696(m), 563(m). Elemental analysis calcd. (%) for $Al_8Fe_3Cl_6C_{104}N_{12}O_{38}H_{132}$ (MW 2754.30): C 45.35, N 6.10, H 4.83; found C 42.24, N 7.91, H 4.67. Elemental analysis calcd. (%) for $Al_8Co_3Cl_7C_{108}N_8O_{38}H_{132}$ (MW 2791.06): C 46.48, N 4.01, H 4.77; found C 46.14, N 6.64, H 5.75. Elemental analysis calcd. (%) for $Al_8Ni_3Cl_8C_{104}N_{12}O_{36}H_{124}$ (MW 2617.34): C 47.73, N 6.42, H 4.78; found C 45.76, N 7.65, H 4.75.

Elemental analysis calcd. (%) for $Al_8Fe_3Br_7C_{104}N_{12}O_{36}H_{124}$ (MW 3057.71): C 40.85, N 5.50, H 4.09; found C 41.73, N 6.63, H 3.33.

Synthesis of AlOC-155

A mixture of aluminum isopropoxide (204 mg, 1 mmol), 3-Chloroisonicotinic acid (240 mg, 1.52 mmol), Iron (III) chloride anhydrous (60 mg, 0.37 mmol), methylamine ethanol solution (40 %, 120 μL), n-butanol (2.5 mL) and DMF (2.5 mL) was sealed in a 20 mL vial and transferred to a preheated oven at 100 °C for 4 days. When cooled to room temperature, red crystals were obtained. (yield: 52 % based on $Al(O^iPr)_3$). The crystals are rinsed with DMF and preserved under a sealed and dry environment. **AlOC-155**-FT-IR (KBr, cm^{-1}): 3433(s), 2955(w), 2880(w), 1666(m), 1628(s), 1481(m), 1597(m), 1443(s), 1330(w), 1275(w), 1157(w), 1099(m), 1055(w) 846(w), 789(m), 673(m), 560(s). Elemental analysis calcd. (%) for $Al_8Fe_3Cl_{19}C_{104}N_{12}O_{36}H_{112}$ (MW3162.99): C 39.49, N 5.31, H 3.57; found C 38.60, N 6.85, H 4.01.

X-ray Crystallographic Analyses

Crystallographic data of crystal **AlOC-151**, **AlOC-152**, **AlOC-154** and **AlOC-151'** were collected on Hybrid Pixel Array detector equipped with Ga-Kα radiation (λ=1.3405 Å) at about 293K, as well as **AlOC-150**, **AlOC-153**, **AlOC-155**, **I_2@ AlOC-151**, **I_2@ AlOC-155**, and **AlOC-155'** was at 100K. The structures were solved with the dual-direct methods using ShelxT and refined with the full-matrix least-squares technique based on F^2 using the SHELXL.[2] Non-hydrogen atoms were refined anisotropically. Hydrogen atoms were added theoretically, riding on the concerned atoms and refined with fixed thermal factors. And n-butyl alcohol molecules are severely disordered and the related hydrogen atoms were not included. All absorption corrections were performed using the multi-scan program. In the crystal data after iodine adsorption, the large peaks of electron density within the pores were identified as iodine. Unfortunately, due to the disorder and poor crystal quality caused by high-temperature iodine steam treatment of the sample, wR_2 value is high, but there is no problem with the crystal data before treatment, so we are confident that the data after iodine adsorption is valid. The obtained crystallographic data are summarized in Table S8-S11.

Reference:

1. W.-W. Wendlandt, H.-G.Hecht, *Reflectance Spectroscopy;* Interscience: New York, 1966.
2. G.-M. Sheldrick, *Acta Crystallogr A Found Adv* 2015**, 71** (Pt 1), 3-8.

2.The structure information for porous materials

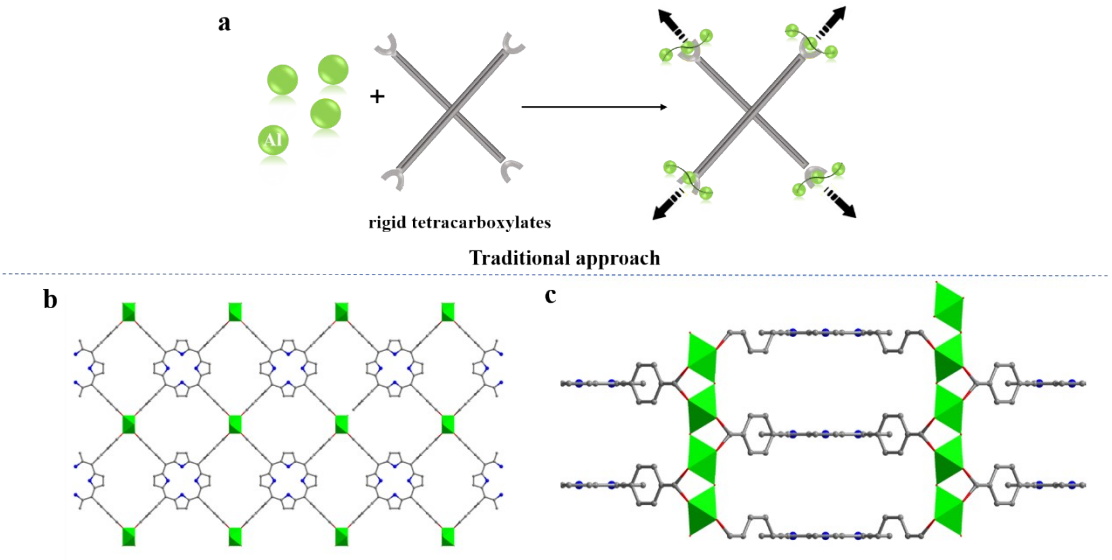

Fig. S1. (a) Traditional approach employing aluminum ions and rigid tetracarboxylic acid ligand.[1] (b) Perspective view of Al-PMOF linked by meso-tetra(4-carboxyl-phenyl) porphyrin ligand along the [010] direction. (c) Perspective view of Al-PMOF along the [001] direction.

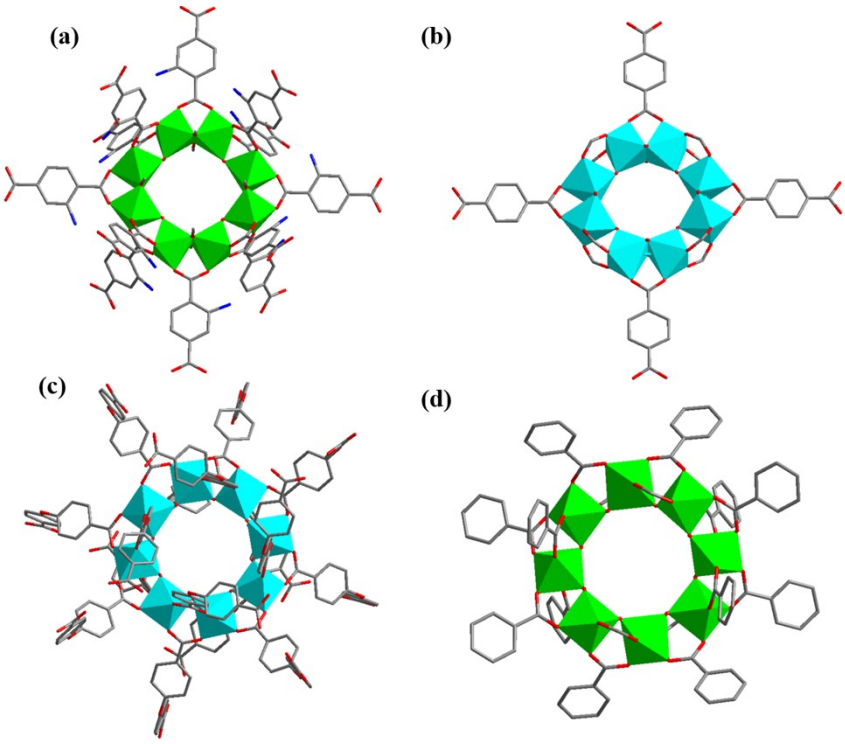

Fig. S2. The edge- and corner-sharing arrangement of the eight octahedral: (a) in CAU-1, (b) in MIL-125. The corner-sharing arrangement of the eight octahedral (c) in FIR-125, (d) in MOF-520. H_3BTB is reduced to benzene for clarity. Color codes: Al, green; Ti, cyan; C, gray; N, blue; O, red.

Table S1. The representative 3D frameworks containing aluminum.

Compounds	Nodes/linker	Topology/Schläfli symbol	reference
CAU-1	$\{Al_8(OH)_4(OCH_3)_8\}^{12+}$ 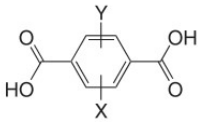	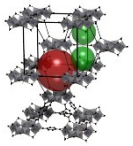 *fcu*	[2]
CAU-3	$[Al_{12}(OCH_3)_{24}]^{12+}$ 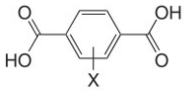	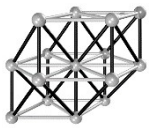 *fcu*	[3]
CAU-21-BPDC	$Al_8(OH)_8(COO)_{16}$ 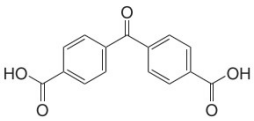	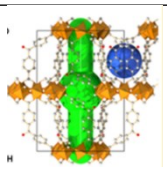 *bcu*	[4]
MIL-53	infinite chains of $AlO_4(OH)_2$ 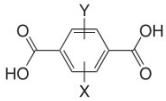	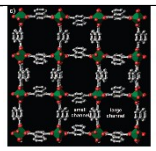 -/-	[5]
MIL-68	infinite chains of $AlO_4(OH)_2$ 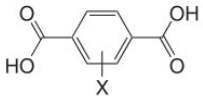	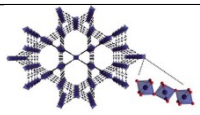 -/-	[6]
MIL-101-NH_2	$[Al_3O(H_2O)_2(OH)]$ 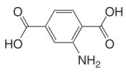	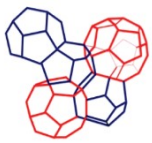 *MTN*	[7]
Al-PMOF	infinite chains of $AlO_4(OH)_2$ 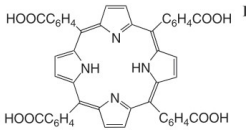	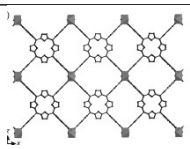 -/-	[1]
MOF-303	$\{AlO_6\}$ 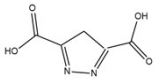	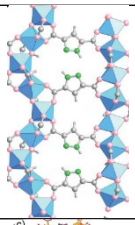 *xxh*	[8]
MOF-519	$Al_8(OH)_8(BTB)_4(H_2BTB)_4$	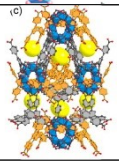 *sum*	[9]

	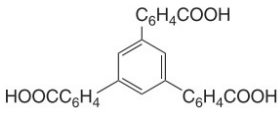		
MOF-520	$Al_8(OH)_8(BTB)_4(HCOO)_4$ 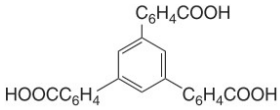	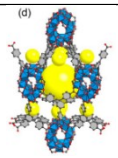 *sum*	[10]
MOF-523	$\{AlO_6\}$ 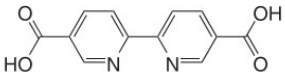	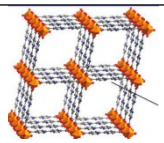 -/-	[11]
AlOC-81	$Al_{10}(INA)_{10}(OEt)_{20}$ 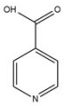	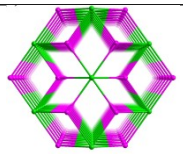 *flu*	[12]

Table S2. The representative 3D frameworks that form by eight-membered ring.

Compound	The arrangement of eight-membered ring	linker	Topo logy	reference
Cau-1	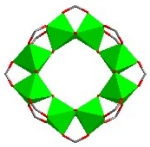	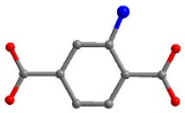	*fcu*	[2]
MOF-519	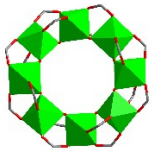	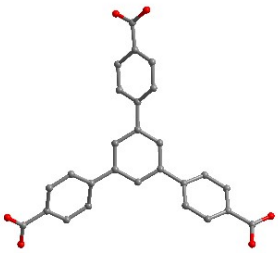	*sum*	[9]
MOF-520				[10]
CAU-21-BPDC	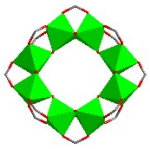	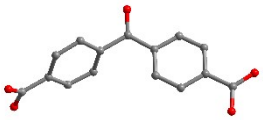	*bcu*	[4]
MIL-125	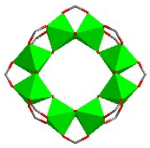	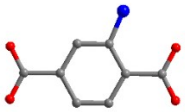	-	[13]

FIJ-125		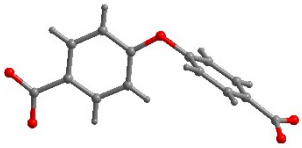	*bcu*	[14]
MIP-207		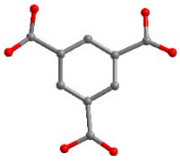	-	[15]
AlOC-150		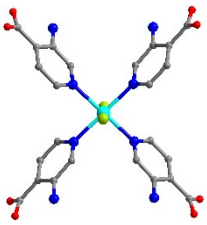	*scu*	This work
AlOC-151		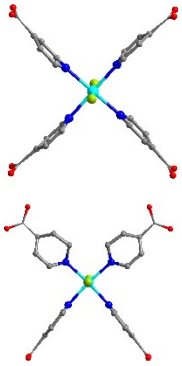	*ftw*	This work

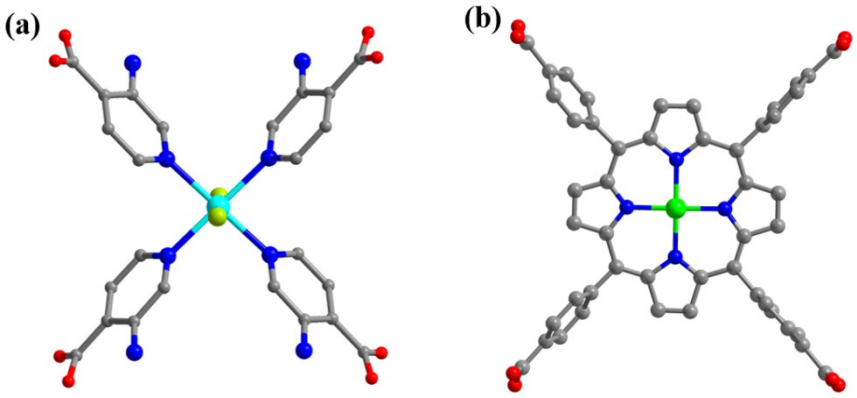

Fig. S3. (a) flexible pseudo-tetracarboxylic acid ligand in **AlOC-150**; (b) rigid metalloporphyrin carboxylic ligands. Color codes: Ti, green; Fe, cyan; C, gray; N, blue; O, red.; Cl, lime.

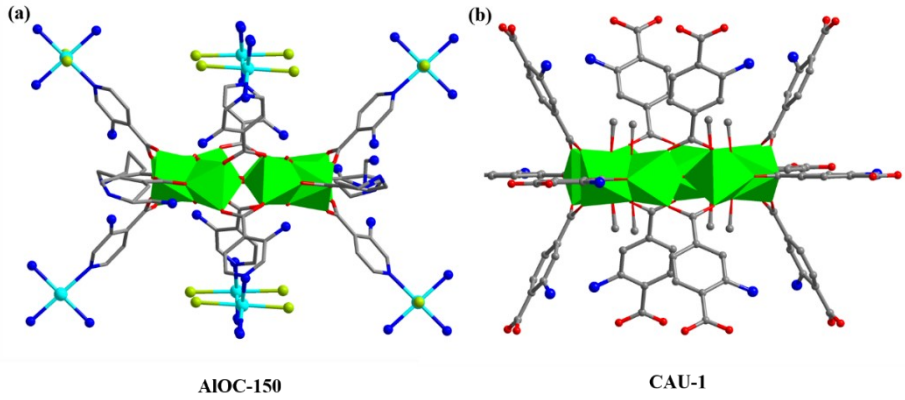

Fig. S4. (a) The 8-connected Al_8 ring in **AlOC-150**; (b) the 12-connected Al_8 ring in CAU-1.

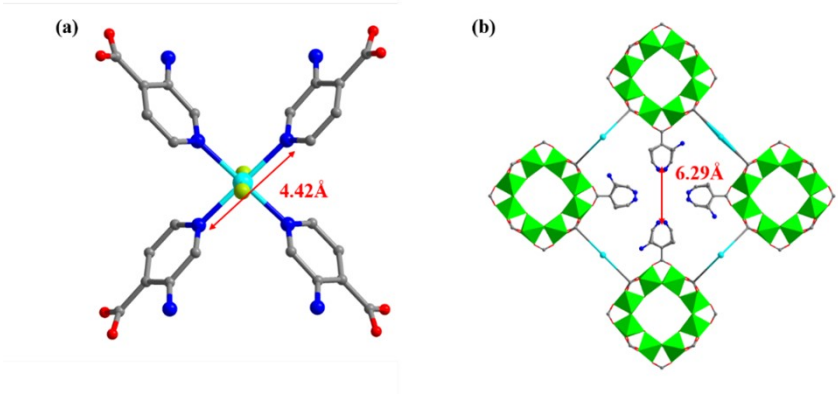

Fig. S5. the distance of N···N (a) in PT-cis linkers; (b) in breaking PT linkers.

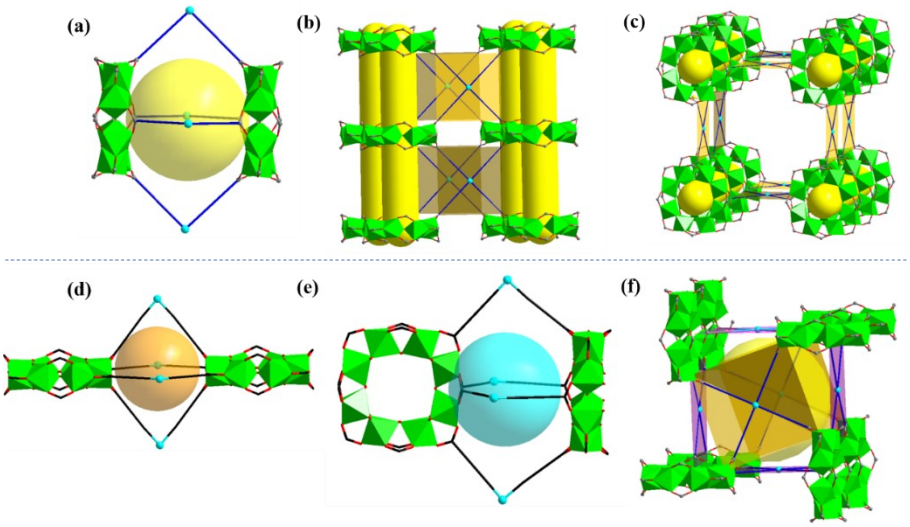

Fig. S6. (a) octahedral cage; (b) nanotubes (side view); (c) nanotubes (top view) in **AlOC-150**; (d) octahedral cage; (e) novel basket-type cage; (f) tetragonal cage in **AlOC-151**. The cage I consist of an octahedral cage containing two neck-and-neck Al_8 rings (13.83 Å × 17.56Å × 8.15 Å) (orange ball), cage Π is a basket-type cage made up of two vertical Al_8 rings (15.69 Å × 18.57Å × 10.63Å) (blue ball), while cage III is a tetragonal cage surrounded by eight Al_8 rings (15.78 Å × 15.78Å × 18.31 Å) (yellow ball). Color codes: Al, green; C, gray; N, blue; O, red.

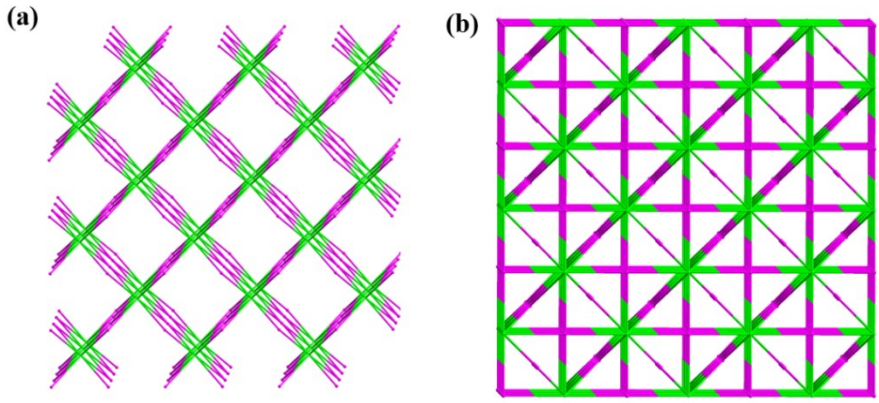

Fig. S7. (a) ***scu*** topology for **AlOC-150**; (b) ***ftw*** topology for **AlOC-151**. Color codes: Al, green; C, gray; N, blue; O, red.

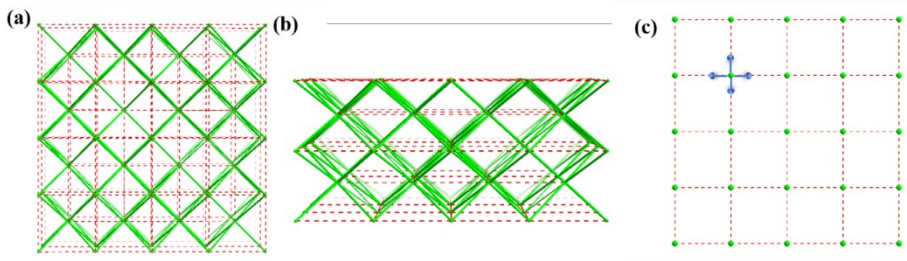

Fig. S8. (a) top view; (b) side view of ***scu*** topology transform to ***ftw*** topology; (c) the position of N on the IN ligands. The red dotted line represents the connection of the decorated IN ligands. Color codes: Al, green; C, gray; N, blue; O, red.

3. PXRD spectra of porous materials

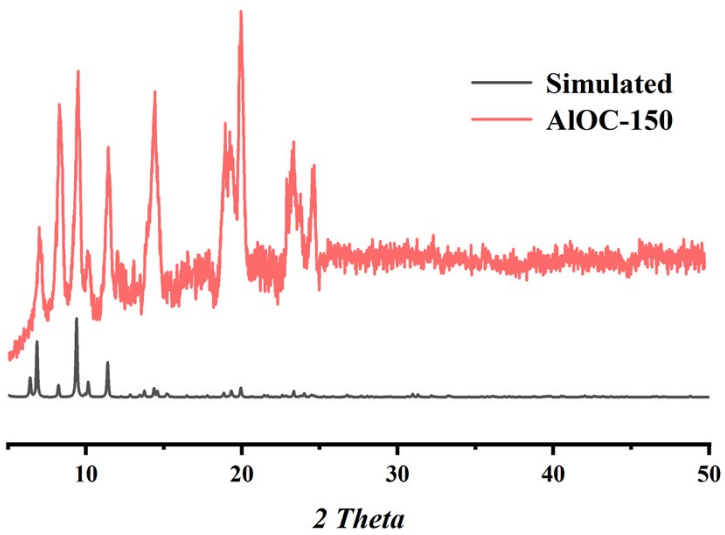

Fig. S9. Simulated single-crystal PXRD patterns (black) and experimental PXRD patterns (red) of **AlOC-150**. The first two narrow peaks fused into one broad peak even though the crystals were selected one by one by hand.

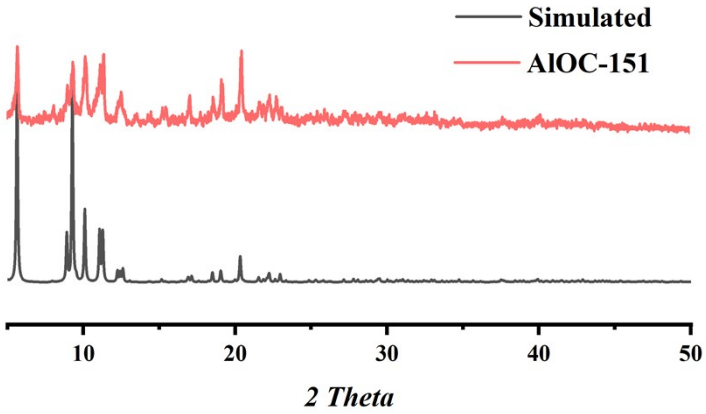

Fig. S10. Simulated PXRD patterns (black) and experimental PXRD patterns (red) of **AlOC-151.**

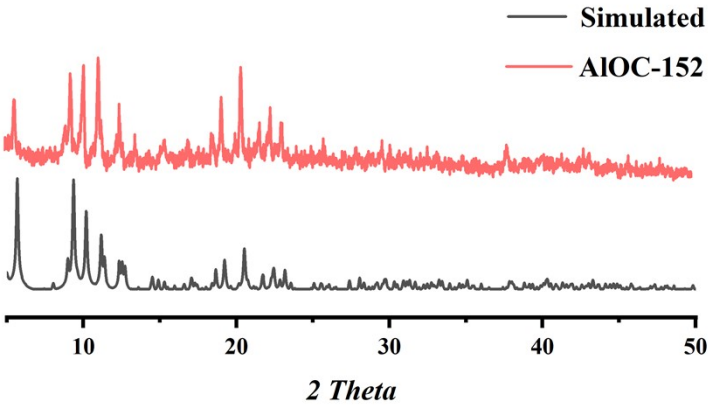

Fig. S11. Simulated PXRD patterns (black) and experimental PXRD patterns (red) of **AlOC-152**.

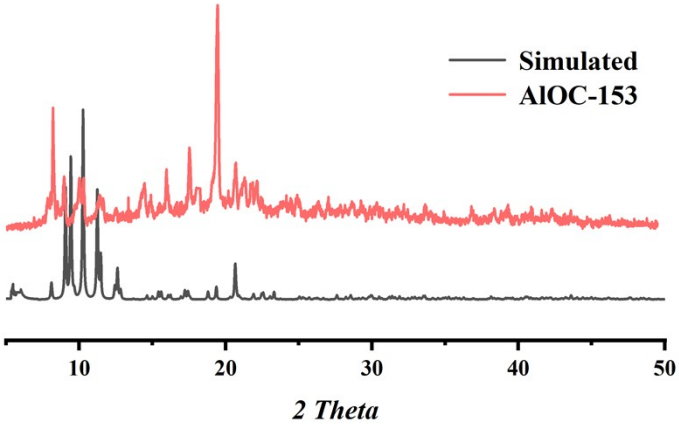

Fig. S12. Simulated PXRD patterns (black) and experimental PXRD patterns (red) of **AlOC-153**.

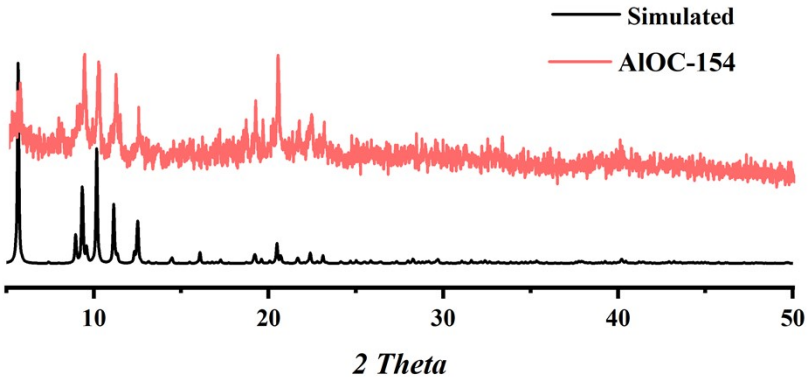

Fig. S13. Simulated PXRD patterns (black) and experimental PXRD patterns (red) of **AlOC-154**.

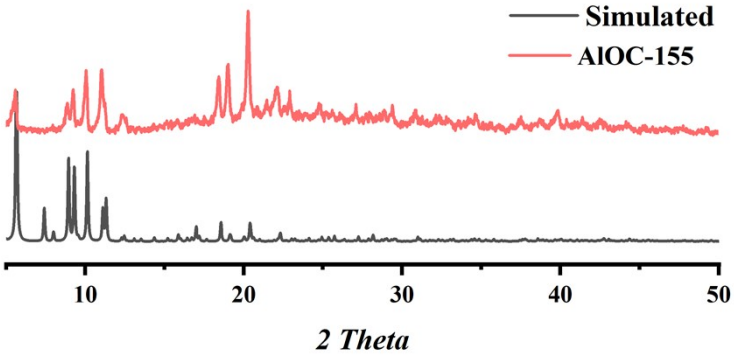

Fig. S14. Simulated PXRD patterns (black) and experimental PXRD patterns (red) of **AlOC-155**.

4. Massive production.

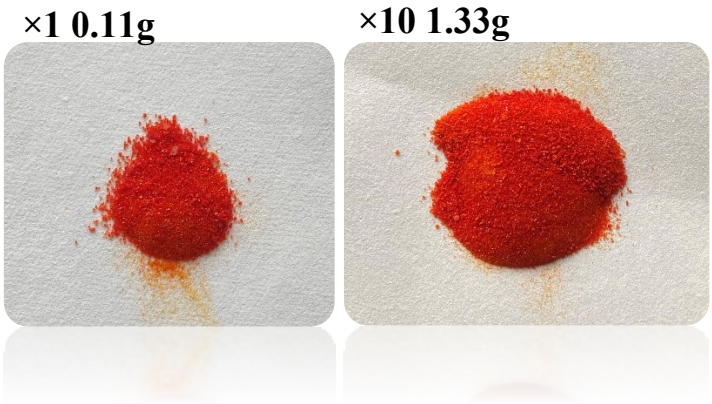

Fig. S15. Massive production of **AlOC-151**.

5. Stability of porous materials

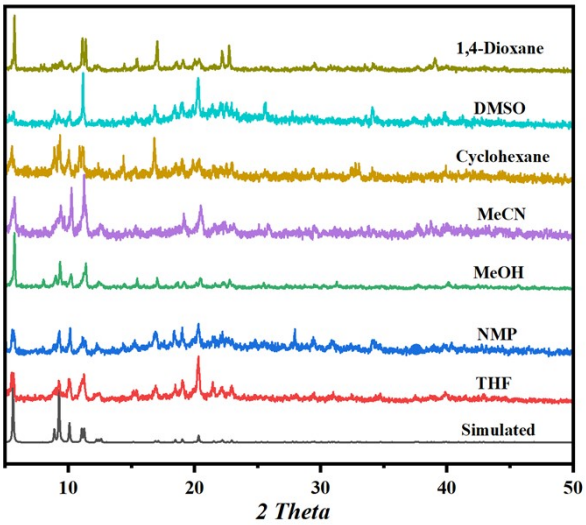

Fig. S16. PXRD patterns of **AlOC-151** in different organic solvents at room temperature for 24 h.

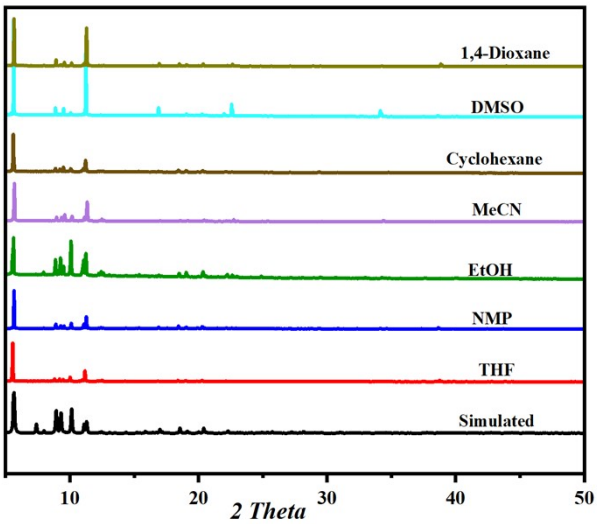

Fig. S17. PXRD patterns of **AlOC-155** in different organic solvents at room temperature for 24 h.

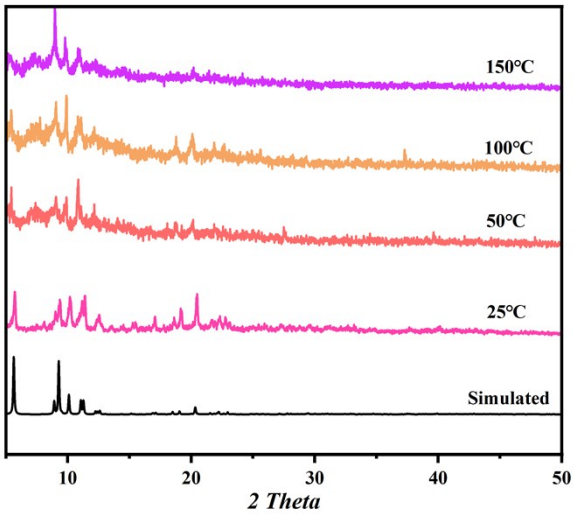

Fig. S18. The Temperature-dependent PXRD patterns of **AlOC-151**.

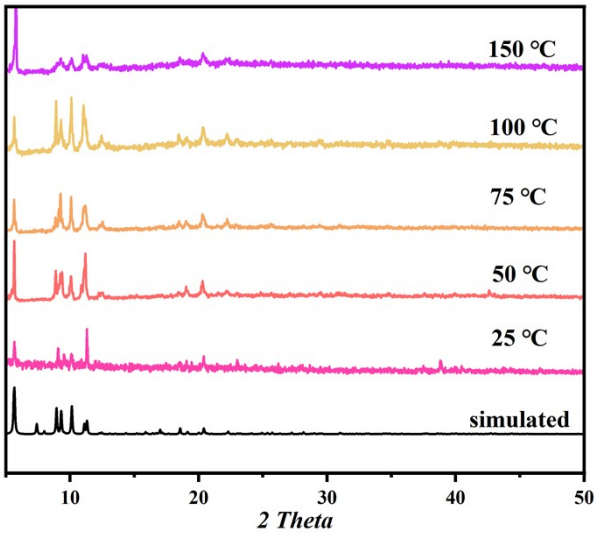

Fig. S19. The Temperature-dependent PXRD patterns of **AlOC-155**.

6. TGA test for porous materials

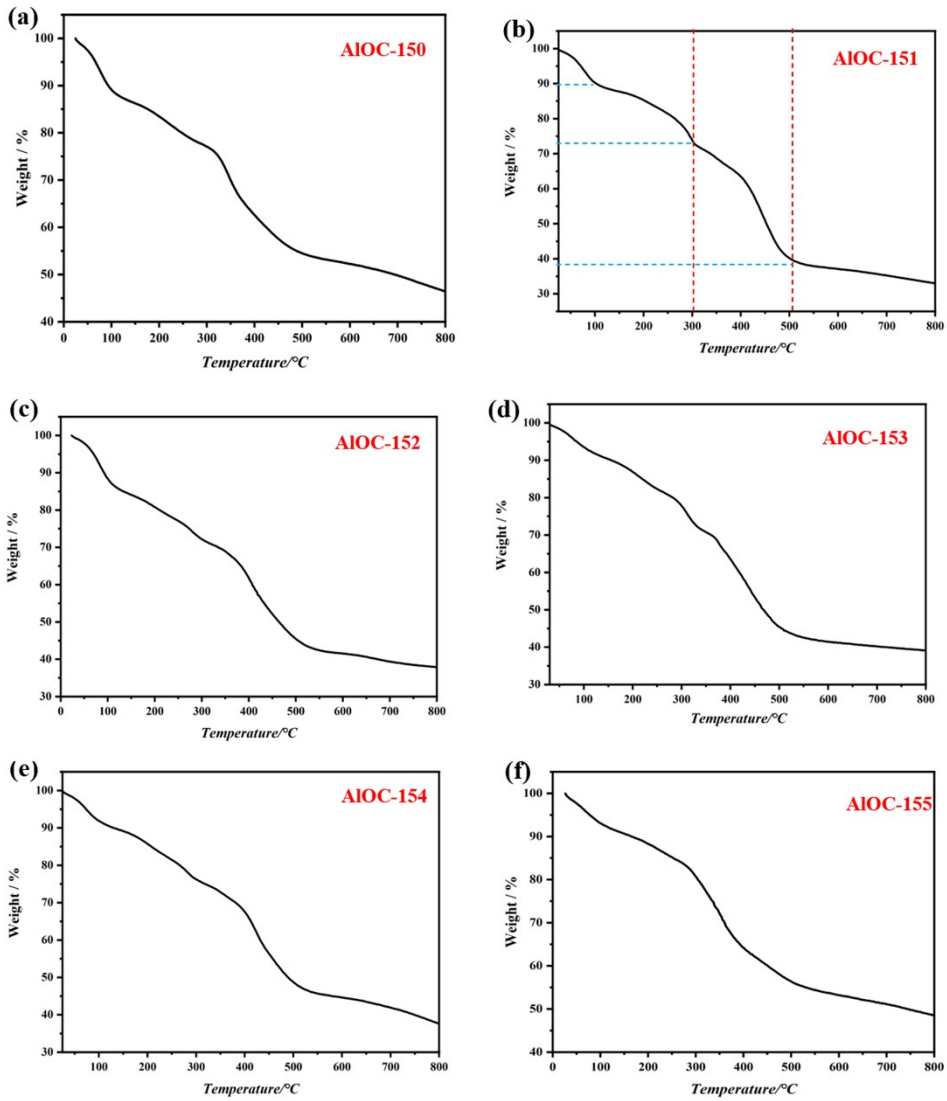

Fig. S20. The TGA curve of **AlOC-150** to **AlOC-155**.

The thermal stability of **AlOC-150** to **AlOC-155** was investigated in N_2 atmosphere up to 800 °C with a heating rate of 10 K min^{-1}, which is presented in Fig. S20. There are similar structures and compositions in **AlOC-150** to **AlOC-155**, so only the TG investigation of **AlOC-151** was described in detail. It reveals a weight loss (10%) between 25 and 100 °C and is assigned to the removal of incorporated water from the pores of the framework. Then weight loss (17.3%) around 306 °C can be attributed to the removal of DMF. The third weight loss (32.5%) between 306 and 501 is assigned to the departure of the organic ligand owning to degradation of the structure.

7. EDS spectra of porous materials

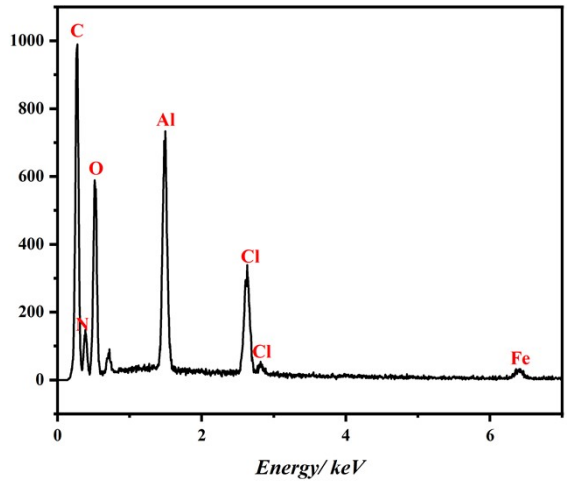

Fig. S21. The EDS spectrum of compound **AlOC-150**.

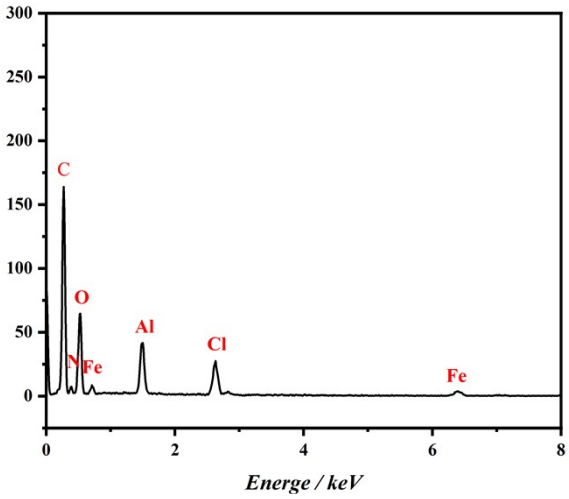

Fig. S22. The EDS spectrum of compound **AlOC-151**.

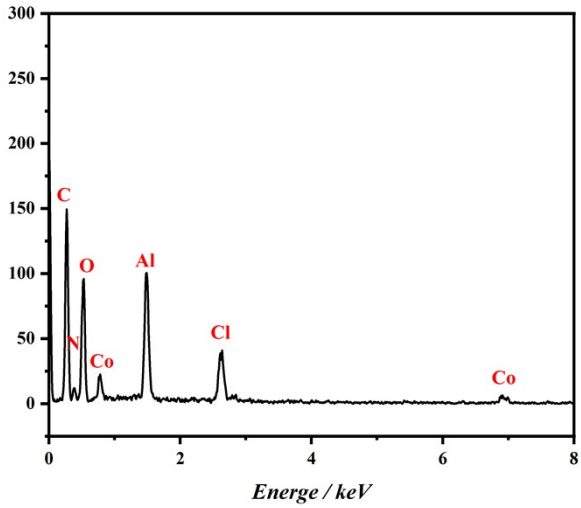

Fig. S23. The EDS spectrum of compound **AlOC-152**.

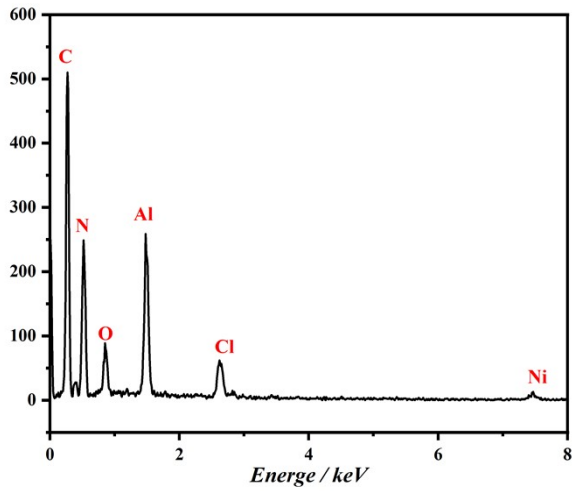

Fig. S24. The EDS spectrum of compound **AlOC-153**.

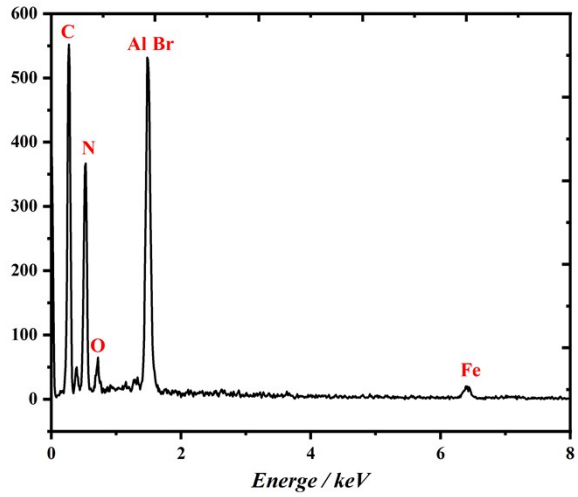

Fig. S25. The EDS spectrum of compound **AlOC-154**.

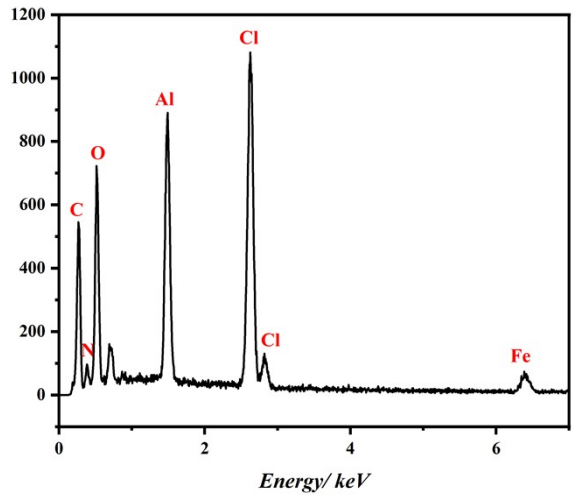

Fig. S26. The EDS spectrum of compound **AlOC-155**.

8. FT-IR spectra of porous materials

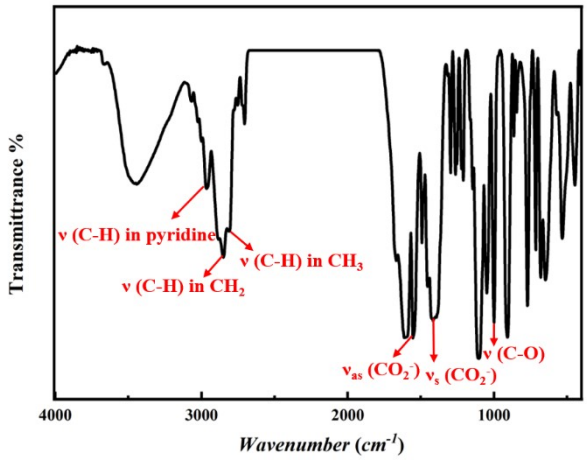

Fig. S27. IR spectrum of **AlOC-150**.

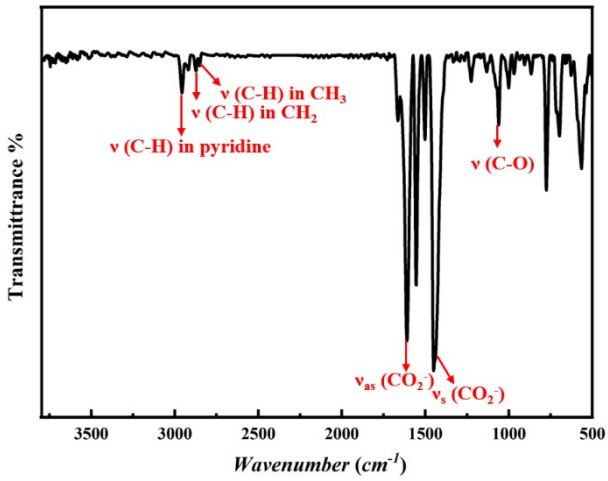

Fig. S28. IR spectrum of **AlOC-151**.

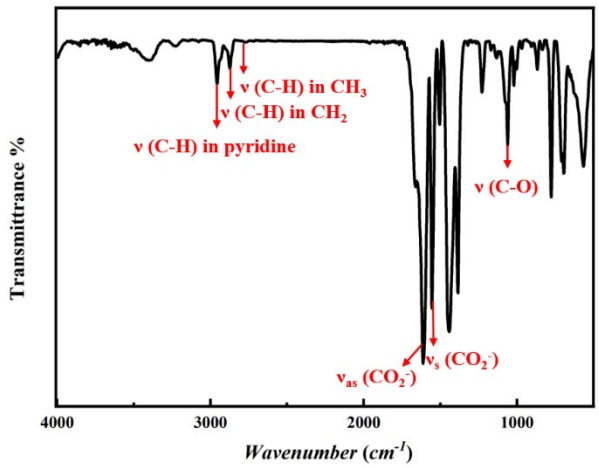

Fig. S29. IR spectrum of **AlOC-152**.

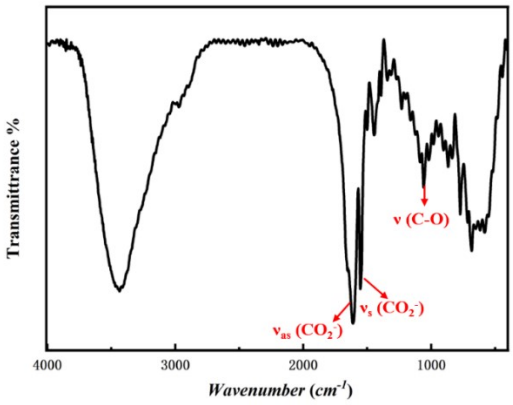

Fig. S30. IR spectrum of **AlOC-153**.

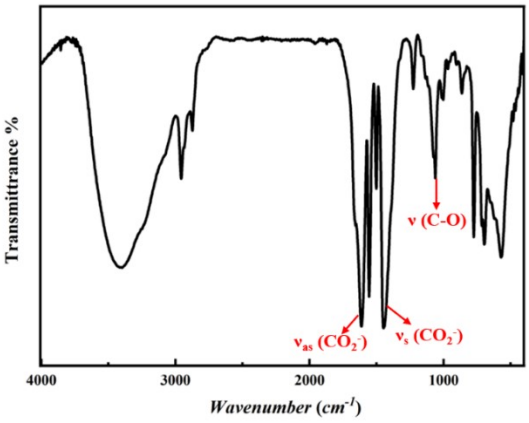

Fig. S31. IR spectrum of **AlOC-154**.

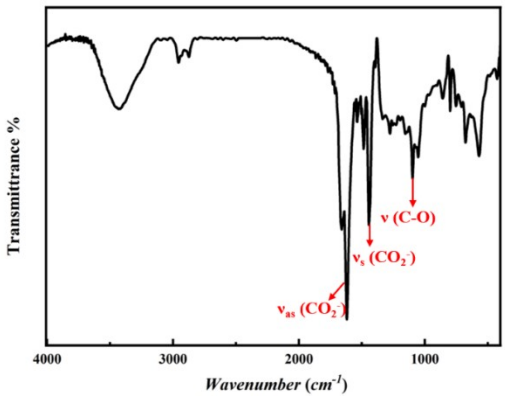

Fig. S32. IR spectrum of **AlOC-155**.

The IR spectra of **AlOC-150** to **AlOC-155** have been recorded in the range of 4000–400 cm^{-1} from solid samples palletized with KBr, which are presented in Fig. S27-S32. In the functional group region ($\nu > 1300$ cm^{-1}), the weak absorption bands at 3087−3063 cm^{-1} are observed, which can be ascribed to the stretching vibration modes of C–H bonds in pyridine rings. On the other hand, the aliphatic C-H stretching-vibrations of the n-butanol oxygen group occur about 3000-2800 cm^{-1}. Moreover, the asymmetric stretching vibration (ν_{as}) and symmetric stretching vibration (ν_s) of the carboxylate group can be clearly attributed, namely, the band at 1610−1560 cm^{-1} is assigned to the ν_{as} (CO_2^-) whilst the signal at 1440−1360 cm^{-1} is ascribed to the ν_s (CO_2^-). In the fingerprint region (1300cm^{-1}>ν > 400 cm^{-1}). The incorporation of 3-Chloroisonicotinic acid in **AlOC-155** is supported by the C-Cl vibrations at 670 cm^{-1}. The typical bands for the NH_2 group at 3497 and 3385 cm^{-1} are not observed in the **AlOC-150** owing to the presence of N-H⋯O hydrogen bonding.

9. Determination of the valence state of metals

Table S3 ICP analysis for porous materials.

		AlOC-151	**AlOC-152**	**AlOC-153**
Wt%	Exp.	Al:6.11%	Al:6.85%	Al:6.09%
		Fe:4.13%	Co:4.77%	Ni:4.57%
	Cal.	Al:7.98%	Al:7.74%	Al:8.40%
		Fe:6.19%	Co:6.34%	Ni:6.85%
Al:M	Exp.	3.0628:1	3.1366:1	2.8989:1
	Cal.	2.6657:1	2.6665:1	2.6676:1

(M=Fe for **AlOC-151**; Co for **AlOC-152**; Ni for **AlOC-153**)

Table S4 BVS analysis for porous materials.

BVS analysis for **AlOC-151**

BVS Value	Bond distance		BVS Value	Bond distance	
Al01	Al01-O1	1.906	Al02	Al02-O3	1.952
3.1602	Al01-O1[1]	1.906	3.1197	Al02-O4[1]	1.873
	Al01-O2	1.942		Al02-O4	1.873
	Al01-O4[1]	1.87		Al02-O6	1.8507
	Al01-O4	1.87		Al02-O7	1.909
	Al01-O5	1.8436		Al02-O7[1]	1.909
Fe01	Fe01-N1	2.233	Fe02	Fe02-N3[7]	2.256
1.9819	Fe01-N1[6]	2.233	1.8938	Fe02-N3	2.256
	Fe01-N2	2.235		Fe02-N3[8]	2.256
	Fe01-N2[6]	2.235		Fe02-N3[9]	2.256
	Fe01-Cl06	2.436		Fe02-Cl05	2.444
	Fe01-Cl06	2.436		Fe02-Cl05	2.444

System code: [1]3/2-Y, 3/2-X, +Z; [6]+X, +Y, 1-Z; [7]2-Y, +X, +Z; [8]2-X, 2-Y, 2-Z; [9]+Y,2-X,2-Z.

BVS analysis for **AlOC-152.**

BVS Value	Bond distance		BVS Value	Bond distance	
Al03	Al03-O00B	1.844	Al04	Al04-O00A	1.952
3.1657	Al03-O00C	1.865m	3.1917	Al04-O00C	1.873
	Al03-O00D	1.896		Al04-O00F	1.873
	Al03-O00E	1.949		Al04-O00G	1.8507
	Al03-O00I[1]	1.912		Al04-O00H[2]	1.909
	Al03-O009	1.869		Al04-O009	1.909
Co01	Co01-Cl05	2.502			
2.1288	Co01-Cl06	2.475			
	Co01-Cl07	2.447			
	Co01-N1[3]	2.163			
	Co01-N1[4]	2.163			
	Co01-N00Z	2.146			

System code: [2]1-X, 1-Y, +Z; [3]-1/2+X, 3/2-Y, 2-Z; [4]-1/2+Y, 3/2-X, +Z.

BVS analysis for **AlOC-153**

BVS Value	Bond distance		BVS Value	Bond distance	
Al01	Al01-O5	1.838	Al02	Al02-O4	1.87
3.2132	Al01-O4[7]	1.861	3.0434	Al02-O4[7]	1.87
	Al01-O4	1.861		Al02-O3	1.942
	Al01-O1	1.899		Al02-O3[7]	1.942
	Al01-O1[7]	1.899		Al02-O7	1.898
	Al01-O2	1.944		Al02-O7[7]	1.898
Ni00	Ni00-Cl08	2.418	Ni01	Ni01-Cl1	2.503
2.2455	Ni00- Cl08[1]	2.418	2.0318	Ni01-Cl07	2.479
	Ni00-N0I	2.064		Ni02-N3	2.120
	Ni00-N0N [2]	2.075		Ni02-N0x[2]	2.120
	Ni00-N0T [3]	2.11		Ni02-N0x [5]	2.120
	Ni00-N011[4]	2.147		Ni02-N0x [6]	2.120

System code: [1]1/2+Y, -1/2+X, 2-Z; [2]1-Y, +X, +Z; [3]1-Y, +X, 2-Z; [4]+X, +Y, 2-Z; [5]1-X, 1-Y, 1-Z; [6]+Y, 1-X, 1-Z; [7]1/2+Y, -1/2+X, +Z;

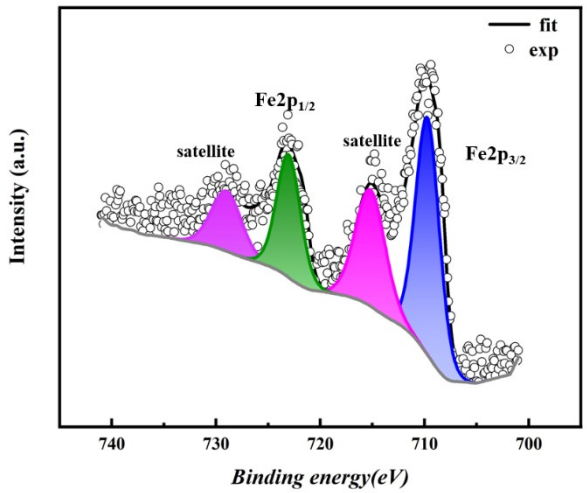

Fig. S33. High-resolution spectrum of Fe 2p for **AlOC-151**.

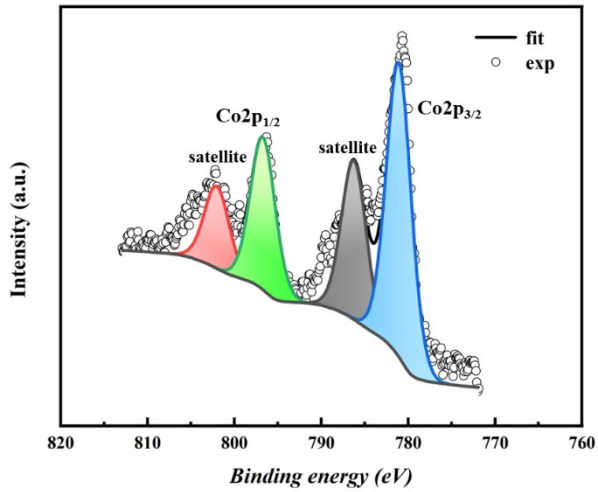

Fig. S34. High-resolution spectrum of Co 2p for **AlOC-152**.

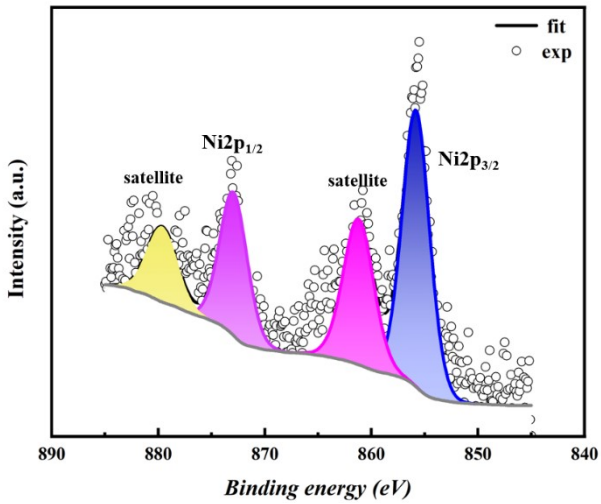

Fig. S35. High-resolution spectrum of Ni 2p for **AlOC-153**.

10. Single-component gas sorption measurement

The gas adsorption isotherms were generated on ASAP 2020 volumetric adsorption equipment. The fresh crystal samples were solvent-exchanged with methanol for **AlOC-151**, ethanol for **AlOC-155** at least 10 times within three days to make sure that the guest solvents were removed. Then the samples were evacuated at 353K for 6 h for **AlOC-151**, instead of at 373K for **AlOC-155**. The sorption measurement was maintained at 77K 273K and 298K under liquid nitrogen, ice slurry and water, respectively.

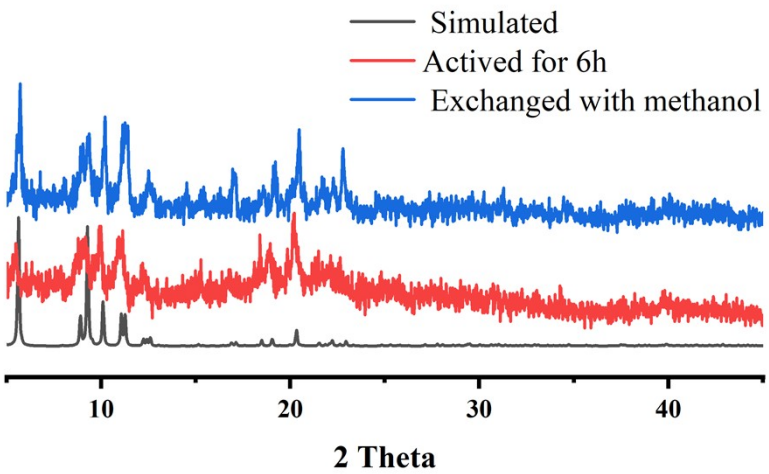

Figure S36. PXRD patterns of **AlOC-151** after methanol exchange and vacuum activation.

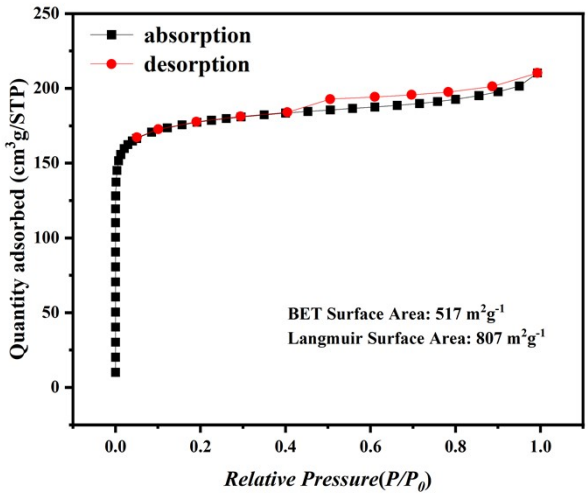

Fig. S37. N_2 isotherm at 77 K of **AlOC-151** after solvent with methanol.

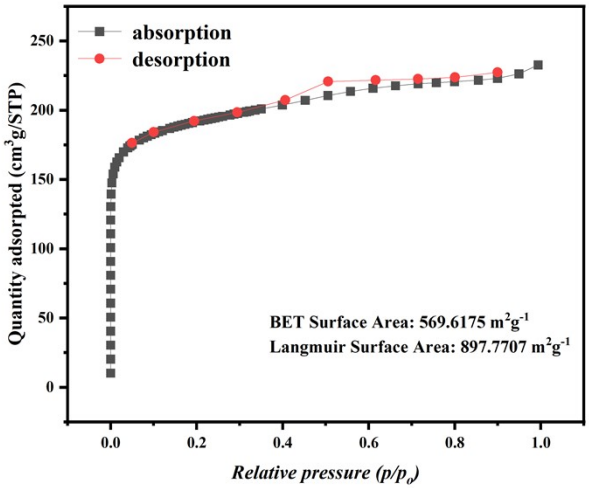

Fig. S38. N_2 isotherm at 77 K of **AlOC-155** after solvent with ethanol.

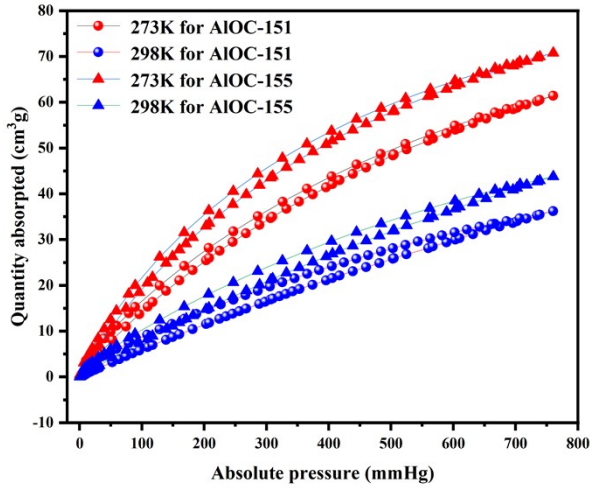

Fig. S39. CO_2 adsorption isotherm at 298 K and 273 K of **AlOC-151** and **AlOC-155**. The overall adsorption effect of **AlOC-155** is better than that of **AlOC-151**.

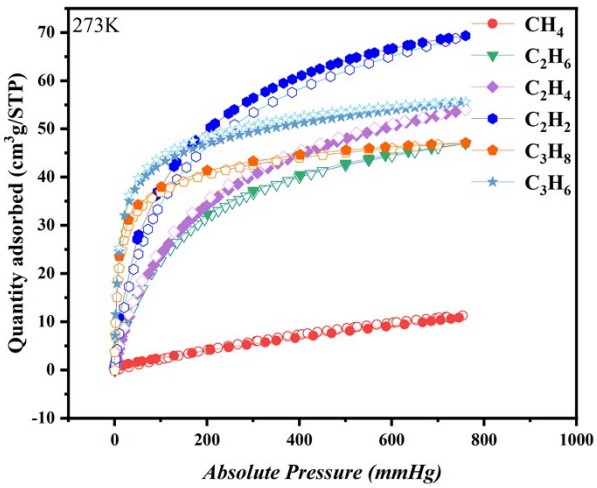

Fig. S40. Light hydrocarbon (CH_4, C_2H_2, C_2H_4, C_2H_6, C_3H_6 and C_3H_8) adsorption isotherms of **AlOC-151** at 273 K.

11. Isosteric heat of gas adsorption

The Clausius-Clapeyron equation was employed to calculate the enthalpies of CO_2 adsorption for **AlOC-151**, a_i and b_i are parameters which are independent of temperature:

$$\ln P = \ln N + \frac{1}{T}\sum_{i=0}^{m} a_i N^i + \sum_{i=0}^{n} b_i N^i$$

Where p is pressure, N is the amount of uptake, T is the temperature and m and n the number of terms required to adequately describe the isotherm.

$$Q_{st} = -R\sum_{i=0}^{m} a_i N^i$$

Where R is the universal gas constant. The coverage dependencies of Q_{st} values were calculated from fitting the adsorption data at different temperatures for **AlOC-151**.

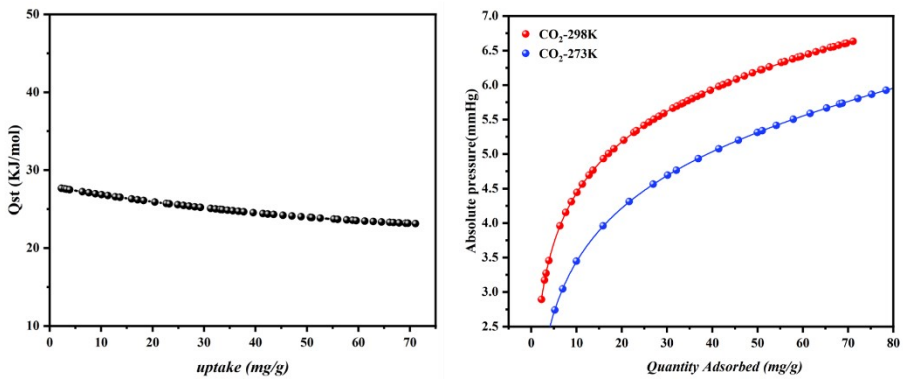

Fig. S41. The isosteric heat of CO_2 adsorption for **AlOC-151** is estimated by the virial equation (left); The CO_2 sorption isotherms for **AlOC-151** fitting by the virial method (right).

12. IAST calculations of adsorption selectivity

In order to evaluate the separation effect of **AlOC-151** on binary mixed-light alkanes, the single-component adsorption isotherms of light alkanes were calculated based on the dual-site Langmuir-Freundlich (DSLF) model. Gas selectivity of mixed C_3H_8/CH_4 (50/50, v/v) and C_3H_6/CH_4 (50/50, v/v) at 298 K were carried out using the ideal adsorbed solution theory (IAST).

$$N = A_1 \frac{b_1 P^{c_1}}{1 + b_1 P^{c_1}} + A_2 \frac{b_2 P^{c_2}}{1 + b_2 P^{c_2}}$$

where P (unit: kPa) is the pressure of the bulk gas at equilibrium with the adsorbed phase, N (unit: mol/kg) is the adsorbed amount per mass of adsorbent, A_1 and A_2 (unit: mmol/g) are the saturation capacities of two different sites, b_1 and b_2 (unit: 1/kPa) is the affinity coefficients of these sites, and c_1 and c_2 represent the deviations from an ideal homogeneous surface.

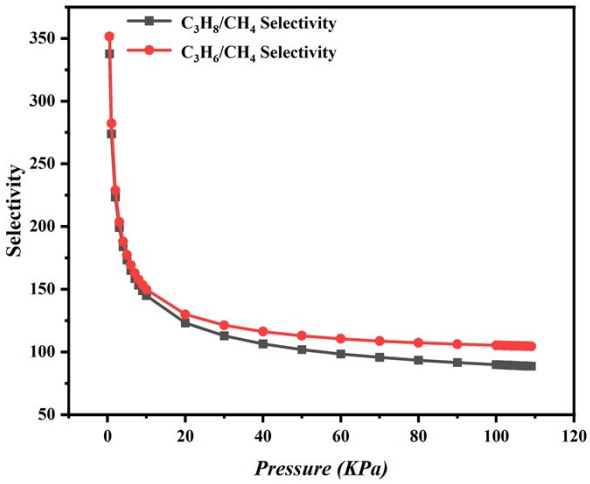

Fig. S42. the IAST selectivity of 50/50 C_3H_8/CH_4 and 50/50 C_3H_6/CH_4 for **AlOC-151** at 298 K, 1 bar.

13. Iodine capture, release and recyclability

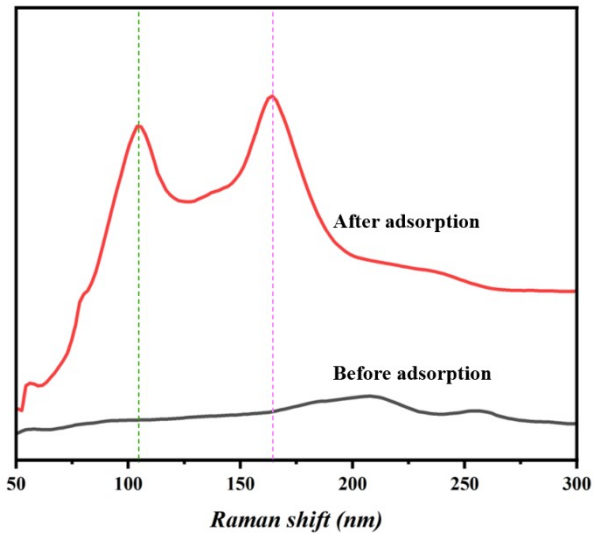

Fig. S43. Comparison of Roman spectrum of **AlOC-151** before and after iodine adsorption.

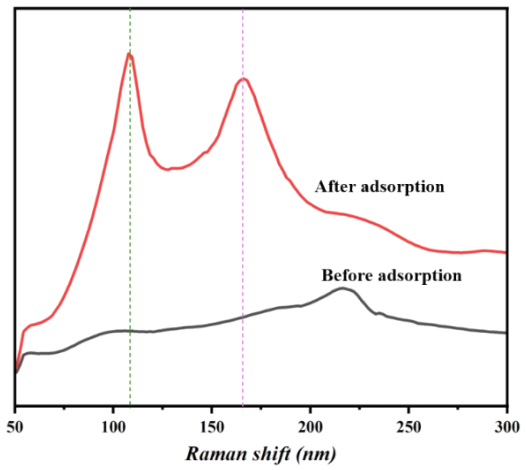

Fig. S44. Comparison of Roman spectrum of **AlOC-155** before and after iodine adsorption (collected with an excitation line of 532 nm at 10% laser power).

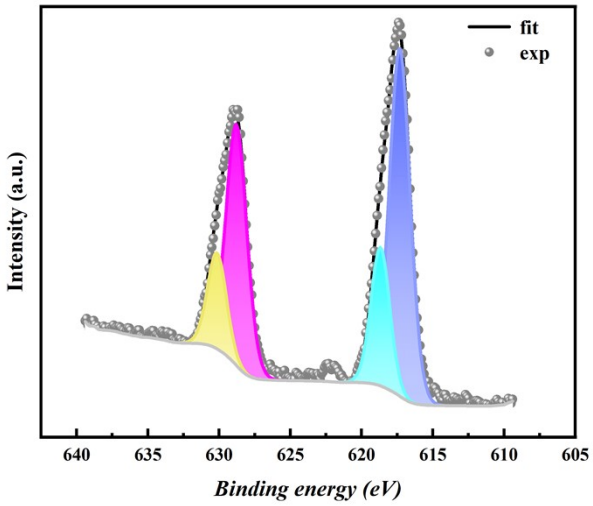

Fig. S45. The high-resolution spectrum of 3d I for **I_2@AlOC-151**.

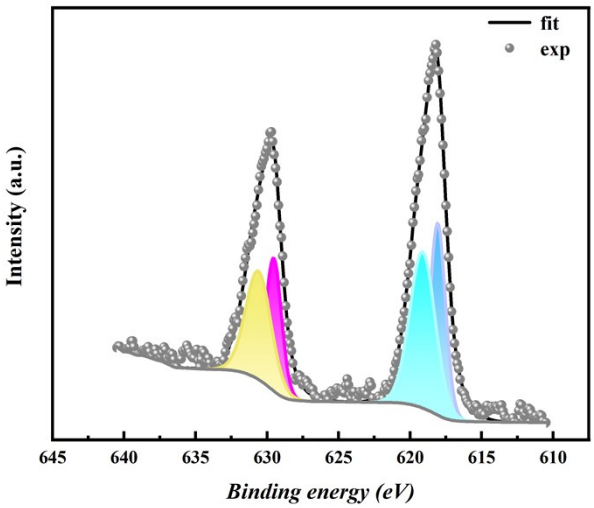

Fig. S46. The high-resolution spectrum of 3d I for **I_2@AlOC-155**.

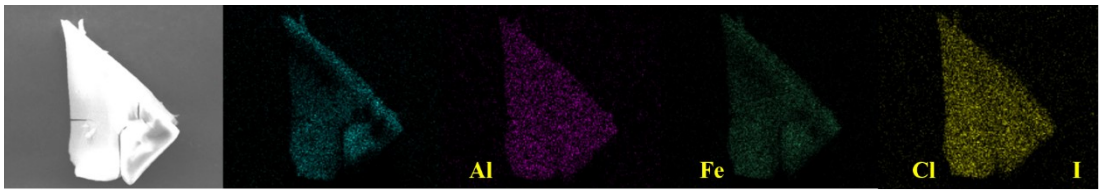

Fig. S47. EDS-mapping spectra of **I_2@AlOC-151**. From left to right are crystal appearance, aluminum, iron, chlorine and iodine elements.

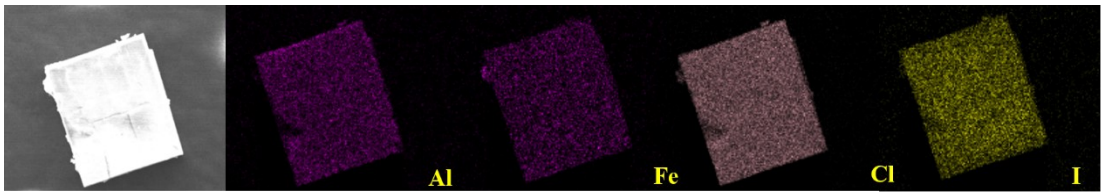

Figure S48. EDS-mapping spectra of **I_2@AlOC-155**. From left to right are crystal appearance, aluminum, iron, chlorine and iodine elements.

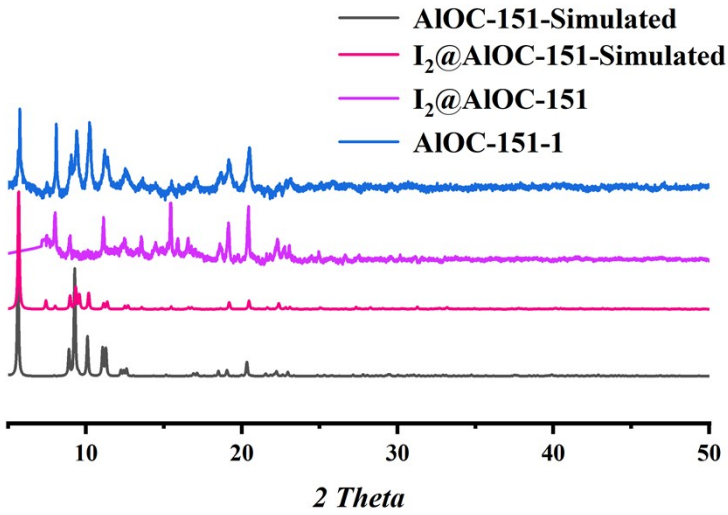

Fig. S49. PXRD patterns of **AlOC-151** after iodine adsorption and release with methanol.

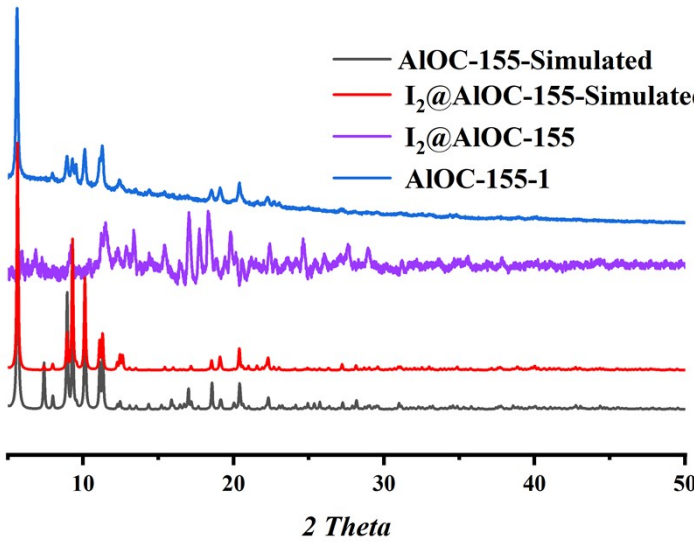

Fig. S50. PXRD patterns of **AlOC-155** after iodine adsorption and release with ethanol.

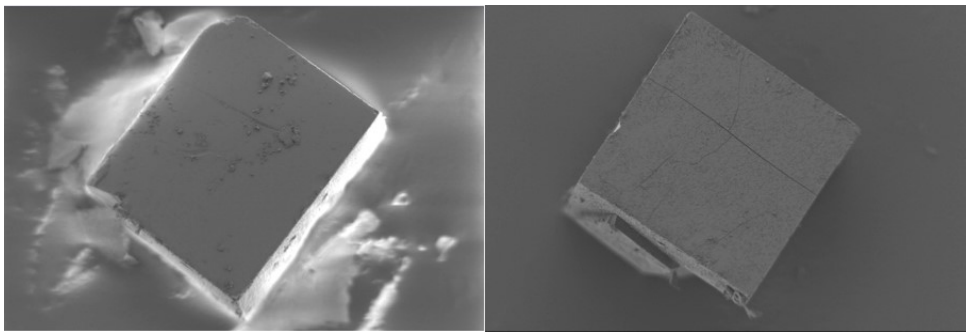

Fig. S51 the SEM imagines before (left) and after (right) iodine adsorption.

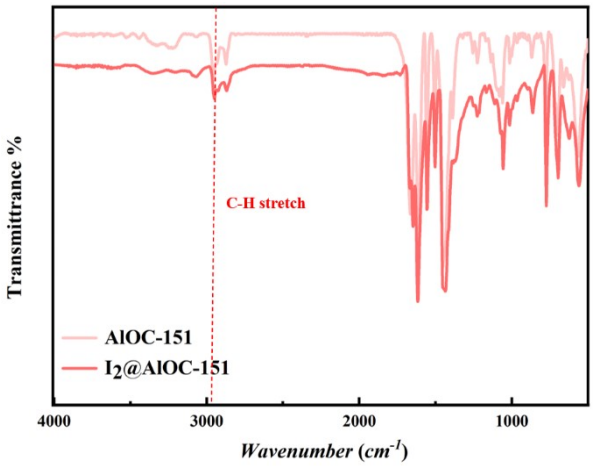

Fig. S52. FT-IR spectra of **AlOC-151** before and after iodine adsorption. the characteristic peak at ~2967.7 cm^{-1} assigned to the C-H on pyridine ring stretching vibration blue shift.

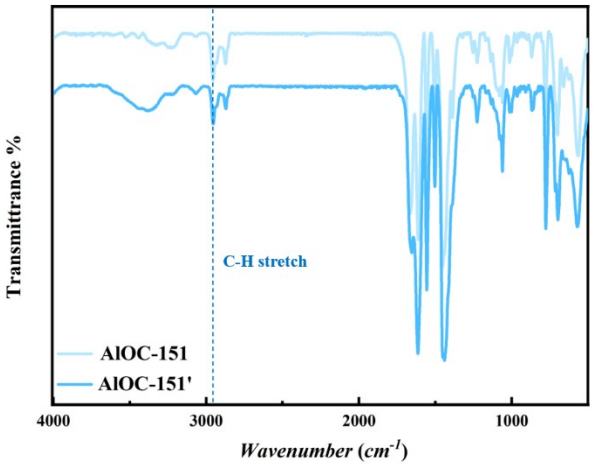

Fig. S53. FT-IR spectra of **AlOC-151** and release with methanol. The absorption peak was restored after release.

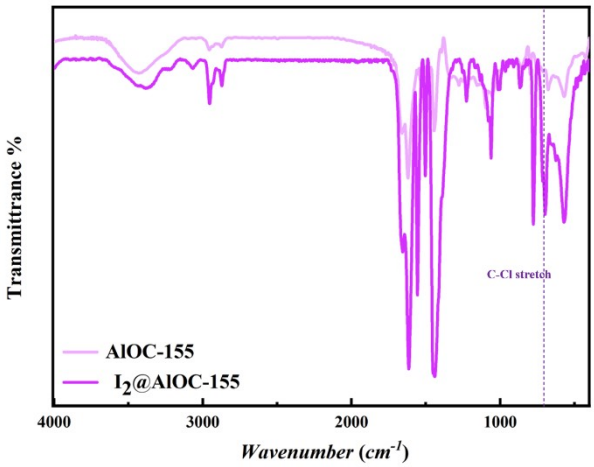

Fig. S54. FT-IR spectra of **AlOC-155** before and after iodine adsorption. the characteristic peak at ~673.1 cm^{-1} assigned to the C-Cl on pyridine ring stretching vibration red shift.

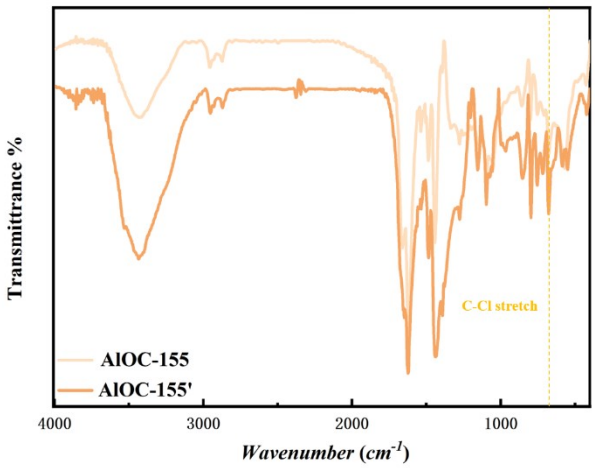

Fig. S55. FT-IR spectra of **AlOC-155** and after release with ethanol. The absorption peak was restored after release.

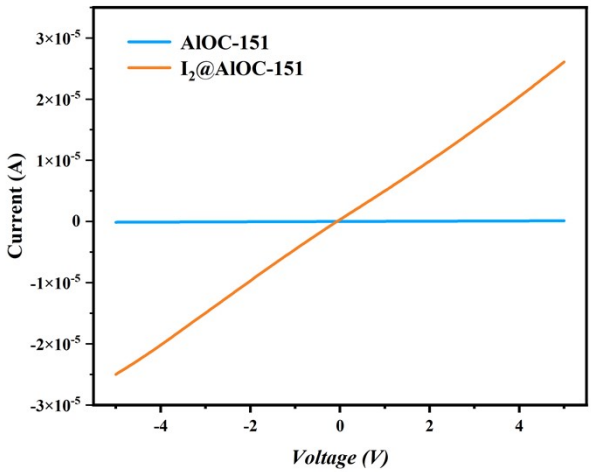

Fig. S56. I-V curves of pristine **AlOC-151** and **I_2@AlOC-151.**

Table S5. BVS analysis of Fe atoms after iodine adsorption.

BVS analysis for **I_2@AlOC-151**

Fe1	Fe1-Cl1	2.279	Fe2	Fe2-Cl2[1]	2.313
2.5777	Fe1-Cl1[1]	2.279	2.4365	Fe2-Cl2	2.314
	Fe1-N1	2.203		Fe2-N2[2]	2.187
	Fe1-N1[5]	2.203		Fe2-N2	2.187
	Fe1-N00s	2.151		Fe2-N2[3]	2.187
	Fe1-N00s[5]	2.151		Fe2-N2[1]	2.187

System code:[1]1-X, 1-Y, -Z; [2]+Y, 1-X, -Z; [3]1-Y, +X, +Z; [5]+X, +Y, 1-Z;

BVS analysis for **I_2@AlOC-155**

Fe0	Fe00-Cl06	2.387	Fe1	Fe1-Cl05	2.429
2.3779	Fe00-Cl06[1]	2.387	2.3521	Fe1-Cl05[5]	2.429
	Fe00-N0F[2]	2.203		Fe1-N0H[6]	2.244
	Fe00- N0F[3]	2.203		Fe1- N0H	2.244
	Fe00-N0G	2.218		Fe1- N0H[3]	2.244
	Fe00-N0G[4]	2.218		Fe1- N0H[7]	2.244

System code: [1]-1/2+Y, 1/2+X, 1-Z; [2]1-Y, +X, 1-Z; [3]1-Y, +X, +Z; [4]+X, +Y, 1-Z; [5]1-X, 1-Y, 2-Z; [6]+X, +Y, 2-Z; [7]+Y, 1-X, 2-Z;

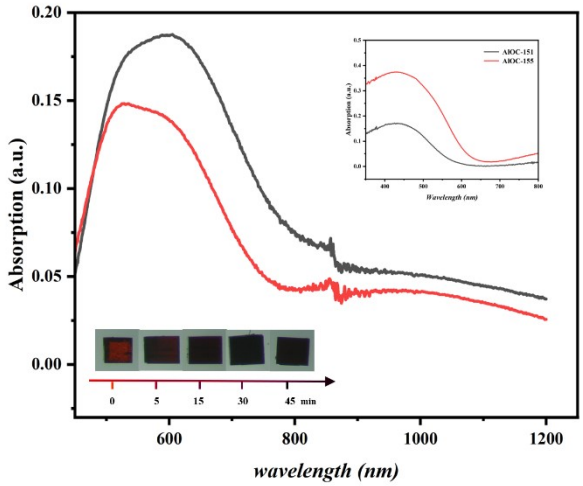

Fig. S57. UV visible spectra of **I_2@AlOC-151** (black line) and **I_2@AlOC-155** (red line); upper right inset: UV visible spectra of **AlOC-151** and **AlOC-155**; lower left inset: photographs showing the visible color change when **AlOC-151** were exposed to I_2 vapor.

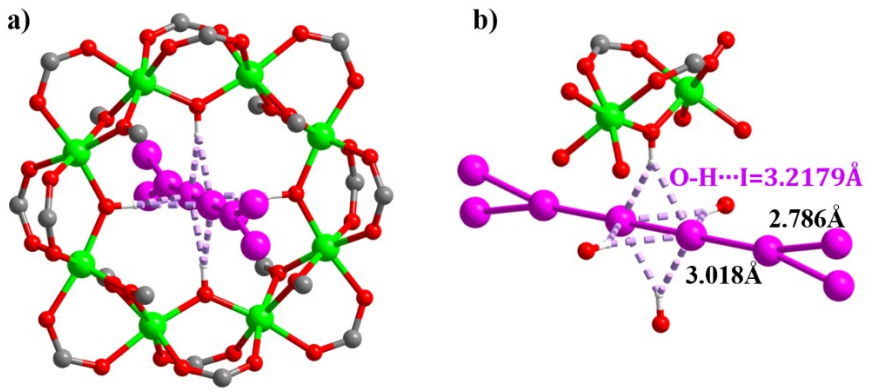

Fig. S58 a) O-H···I interaction and b) the bond length in adsorption site I of **I_2@AlOC-151.** (Color codes: Al, green; Fe, cyan; C, gray; N, blue; O, red. I, pink. Some n-butanol and isonicotinic acid rings are omitted for clarity.

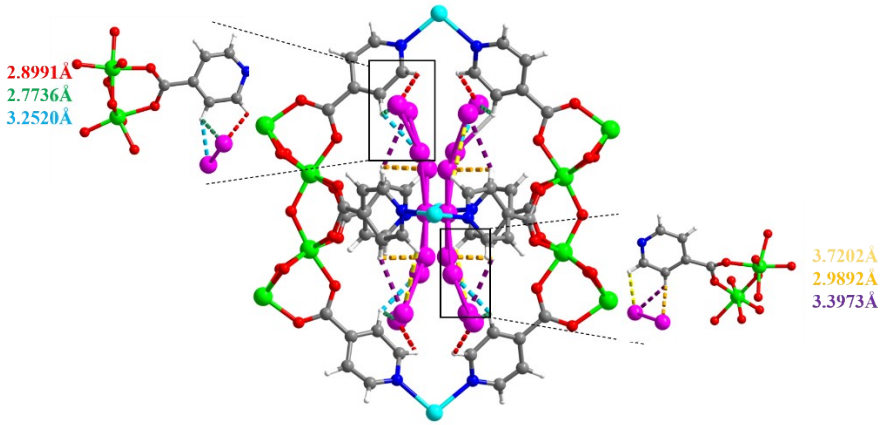

Fig. S59 C-H···I interaction and the bond length in adsorption site II of **I_2@AlOC-151.** (Color codes: Al, green; Fe, cyan; C, gray; N, blue; O, red. I, pink. Some n-butanol and isonicotinic acid rings are omitted for clarity.

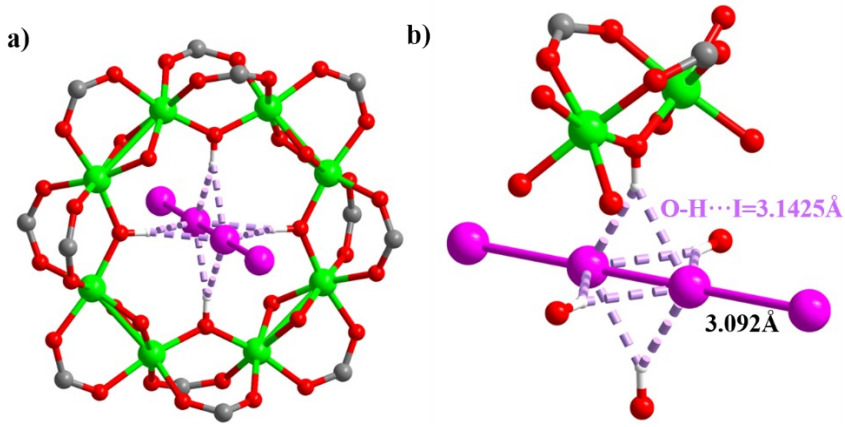

Fig. S60 O-H···I interaction and (b) the bond length in adsorption site I of **I_2@AlOC-155.** (Color codes: Al, green; Fe, cyan; C, gray; N, blue; O, red. I, pink. Some n-butanol and isonicotinic acid rings are omitted for clarity.

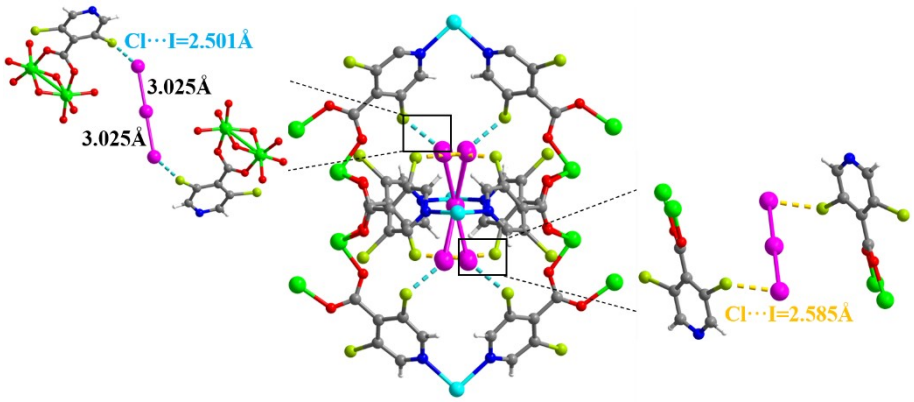

Fig. S61 C-Cl···I interaction and the bond length in adsorption site II of **I_2@AlOC-155.** (Color codes: Al, green; Fe, cyan; C, gray; N, blue; O, red. I, pink. Some n-butanol and isonicotinic acid rings are omitted for clarity.

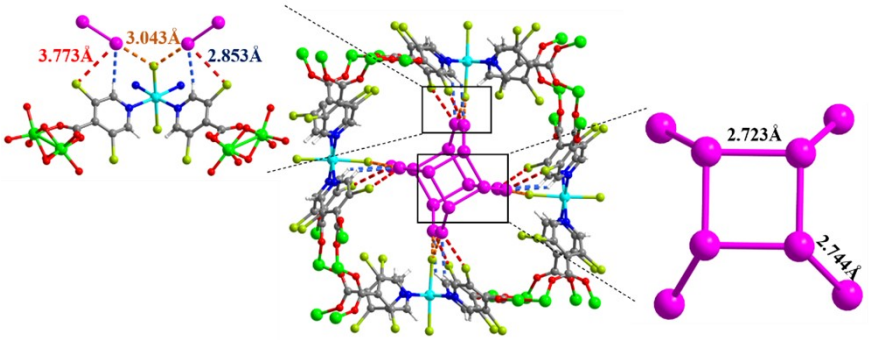

Fig. S62 C-Cl···I, C-H···I interaction and the bond length in adsorption site III of **I_2@AlOC-155.** (Color codes: Al, green; Fe, cyan; C, gray; N, blue; O, red. I, pink. Some n-butanol and isonicotinic acid rings are omitted for clarity.

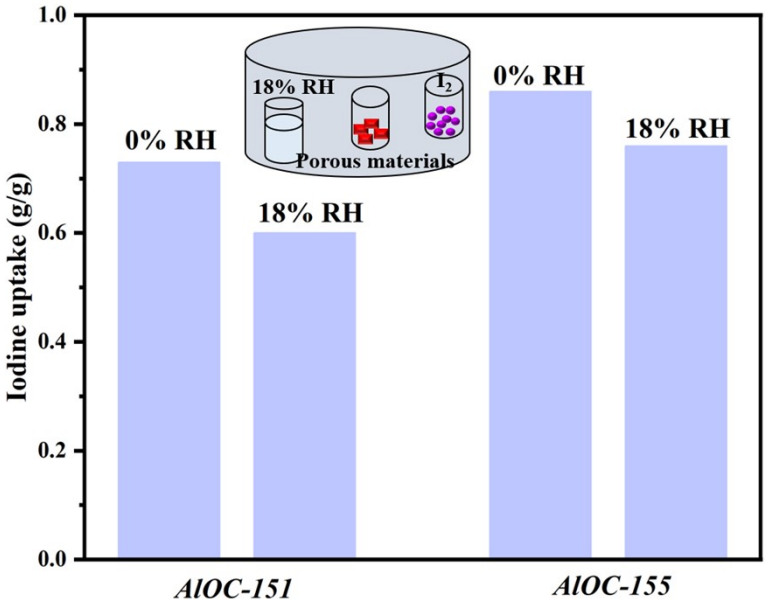

Fig. S63 the Adsorption capacity of porous materials at 80 °C in saturated iodine vapor with 0% RH and 18% RH.

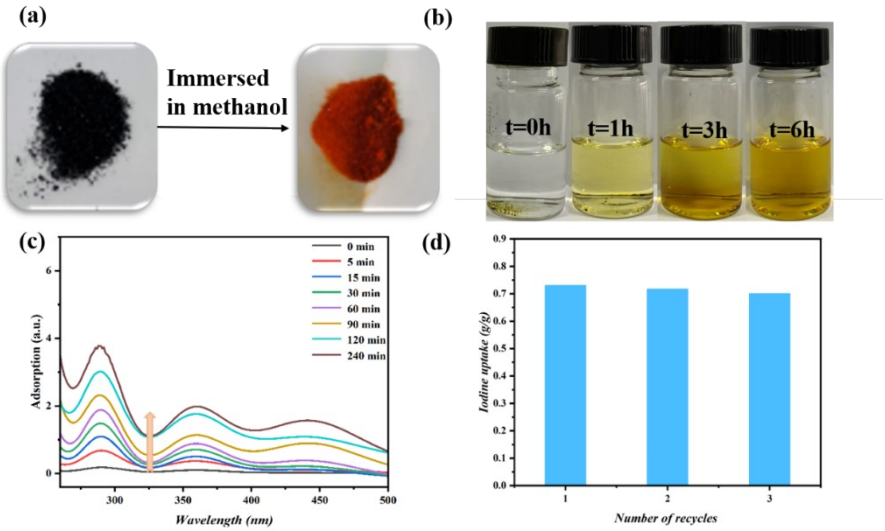

Fig. S64 (a) the photos of Crystal color changes of **AlOC-151** before and after methanol release; (b) photos of the I_2-released process of **I_2@AlOC-151** soaked in methanol; (c) temporal evolution absorbance for the I_2 released from methanol; (d) three times cycle experimental of **AlOC-151**.

14.Crystallography data

Table S6. Comparison of parameters for **AlOC-151** before and after iodine adsorption and release.

	AlOC-151	I_2@AlOC-151	AlOC-151-1
Crystal system	tetragonal	tetragonal	tetragonal
Space group	*P*4/mbm	*P*4/mbm	*P*4/mbm
a [Å]	22.1660(2)	22.0217(4)	22.1414(2)
b [Å]	22.1660(2)	22.0217(4)	22.1414(2)
c [Å]	18.5421(3)	18.4702(5)	18.5120(2)
α [◦]	90	90	90
β [◦]	90	90	90
γ [◦]	90	90	90
V [Å ^{3}]	9110.3(2)	8957.2(4)	9075.35(19)
R_1, wR_2 [I>2σ(I)]	0.0751, 0.2467	0.2154, 0.5111	0.0712, 0.2322
R_1, wR_2 [all data]	0.0853, 0.2587	0.2259, 0.5195	0.0820, 0.2434

Table S7. Comparison of parameters for **AlOC-155** before and after iodine adsorption and release.

	AlOC-155	I_2@AlOC-155	AlOC-155-1
Crystal system	tetragonal	tetragonal	tetragonal
Space group	*P*4/mbm	*P*4/mbm	*P*4/mbm
a [Å]	22.1208(2)	22.1507(10)	22.0492(3)
b [Å]	22.1208(2)	22.1507(10)	22.0492(3)
c [Å]	18.5119(2)	18.5030(2)	18.4944(3)
α [◦]	90	90	90
β [◦]	90	90	90
γ [◦]	90	90	90
V [Å ^{3}]	9058.42(19)	9078.56(13)	8991.4(3)
R_1, wR_2 [I>2σ(I)]	0.0954, 0.2685	0.1844, 0.4761	0.0832, 0.2482
R_1, wR_2 [all data]	0.1111, 0.2829	0.2025, 0.4934	0.0922, 0.2606

Table S8. Experimental single-crystal X-ray data for **AlOC-150**, **AlOC-151** and **AlOC-152**.

	AlOC-150	AlOC-151	AlOC-152
Empirical formula	$Al_8Fe_2Cl_4C_{104}N_{24}O_{43}H_{142}$	$Al_8Fe_3Cl_6C_{104}N_{12}O_{38}H_{132}$	$Al_8Co_3Cl_7C_{108}N_8O_{38}H_{132}$
Formula weight	2885.75	2754.30	2791.06
Temperature / k	100.01(10)	293(2)	293(2)
Crystal system	tetragonal	tetragonal	tetragonal
Space group	*P*4/nbm	*P*4/mbm	*P*4/mbm
a [Å]	27.5493(2)	22.1660(2)	21.99545(17)
b [Å]	27.5493(2)	22.1660(2)	21.99545(17)
c [Å]	12.87900(10)	18.5421(3)	18.3985(2)
α [◦]	90	90	90
β [◦]	90	90	90
γ [◦]	90	90	90
V [Å ^{3}]	9774.70(16)	9110.3(2)	8901.23(17)
Z	2	2	2
ρ_{calcd} [g cm^{-3}]	0.980	1.004	1.041
μ [mm^{-1}]	2.566	2.406	2.730
F (000)	3004.0	2856.0	2888.0
	$-34 \leq h \leq 34$	$-27 \leq h \leq 16$	$-28 \leq h \leq 28$
Index ranges	$-25 \leq k \leq 30$	$-13 \leq k \leq 28$	$-14 \leq k \leq 28$
	$-7 \leq l \leq 15$	$-24 \leq l \leq 23$	$-23 \leq l \leq 23$
Reflections collected	30845	35007	35955
Independent refs [R_{int}]	5141 [0.0280]	5506 [0.0338]	5379 [0.0248]
date/restraints/parameters	5141/84/276	5506/21/239	5379/6/274
Goodness-of-fit on F^2	1.384	1.064	1.074
R_1, wR_2 [I>2σ(I)]	0.0926, 0.2924	0.0751, 0.2467	0.0769, 0.2549
R_1, wR_2 [all data]	0.1019, 0.0.3110	0.0853, 0.2587	0.0797, 0.2591

Table S9. Experimental single crystal X-ray data for **AlOC-153**, **AlOC-154** and **AlOC-155**.

	AlOC-153	AlOC-154	AlOC-155
Empirical formula	$Al_8Ni_3Cl_8C_{104}N_{12}O_{36}H_{124}$	$Al_8Fe_3Br_7C_{104}N_{12}O_{36}H_{124}$	$Al_8Fe_3Cl_{19}C_{104}N_{12}O_{36}H_{112}$
Formula weight	2617.34	3057.71	3162.99
Temperature / k	100.00(10)	100.00(10)	100.00(10)
Crystal system	tetragonal	tetragonal	tetragonal
Space group	*P*4bm	*P*4/mbm	*P*4/mbm
a [Å]	21.8334(3)	22.0664(10)	22.1208(2)
b [Å]	21.8334(3)	22.0664(10)	22.1208(2)
c [Å]	18.3026(5)	18.4584(3)	18.5119(2)
α [◦]	90	90	90
β [◦]	90	90	90
γ [◦]	90	90	90
V [Å ^{3}]	8724.8(3)	8987.88(9)	9058.42(19)
Z	2	2	2
ρ_{calcd} [g cm^{-3}]	0.996	1.130	1.160
μ [mm^{-1}]	3.062	3.088	3.606
F (000)	2680.0	3091.0	3226.0
	$-24 \leq h \leq 25$	$-27 \leq h \leq 28$	$-25 \leq h \leq 20$
Index ranges	$-19 \leq k \leq 28$	$-24 \leq k \leq 28$	$-28 \leq k \leq 27$
	$-23 \leq l \leq 18$	$-23 \leq l \leq 12$	$-23 \leq l \leq 23$
Reflections collected	31843	31137	32144
Independent refs [R_{int}]	8869[0.0761]	5407 [0.0273]	5430 [0.0411]
date/restraints/parameters	8869/220/490	5407/355/282	5430/48/332
Goodness-of-fit on F^2	1.008	1.297	1.092
R_1, wR_2 [I>2σ(I)]	0.0883, 0.2402	0.0851, 0.2800	0.0954, 0.2685
R_1, wR_2 [all data]	0.1246, 0.2714	0.0908, 0.2879	0.1111, 0.2829

Table S10. Experimental single-crystal X-ray data for **I_2@AlOC-151** and **I_2@AlOC-155**.

	I_2@AlOC-151	I_2@AlOC-155
Empirical formula	$Al_8Fe_3Cl_6C_{100}N_{12}O_{36}H_{120}I_{5.5}$	$Al_8Fe_3Cl_{18}C_{104}N_{12}O_{36}H_{116}I_{3.2}$
Formula weight	3360.11	3545.75
Temperature / k	100.01(12)	100.00(10)
Crystal system	tetragonal	tetragonal
Space group	*P*4/mbm	*P*4/mbm
a [Å]	22.0217(4)	22.1507(10)
b [Å]	22.0217(4)	22.1507(10)
c [Å]	18.4702(5)	18.5030(2)
α [◦]	90	90
β [◦]	90	90
γ [◦]	90	90
V [Å ^{3}]	8957.2(4)	9078.56(13)
Z	2	2
ρcalcd [g cm^{-3}]	1.246	1.297
μ [mm^{-1}]	11.056	7.882
F (000)	3335.0	3490.0
Index ranges	$-25 \leq h \leq 25$ $-26 \leq k \leq 26$ $-22 \leq l \leq 18$	$-25 \leq h \leq 28$ $-23 \leq k \leq 28$ $-23 \leq l \leq 23$
Reflections collected	25354	32712
Independent refs [Rint]	4642[0.0902]	5441 [0.0534]
date/restraints/parameters	4642/108/310	5541/127/357
Goodness-of-fit on F^2	2.286	2.303
R_1, wR_2 [I>2σ(I)]	0.2154, 0.5111	0.1844, 0.4761
R_1, wR_2 [all data]	0.2259, 0.5195	0.2025, 0.4934

Table S11. Experimental single-crystal X-ray data for **AlOC-151′** and **AlOC-155′**.

	AlOC-151-1	AlOC-155-1
Empirical formula	$Al_8Fe_3Cl_7C_{104}N_{12}O_{36}H_{120}$	$Al_8Fe_3Cl_{19}C_{104}N_{12}O_{36}H_{112}$
Formula weight	2609.26	3162.99
Temperature / k	293(2)	100.01(10)
Crystal system	tetragonal	tetragonal
Space group	*P*4/mbm	*P*4/mbm
a [Å]	22.1414(2)	22.0492(3)
b [Å]	22.1414(2)	22.0492(3)
c [Å]	18.5120(2)	18.4944(3)
α [◦]	90	90
β [◦]	90	90
γ [◦]	90	90
V [Å ^{3}]	9075.35(19)	8991.4(3)
Z	2	2
ρcalcd [g cm^{-3}]	0.955	1.168
μ [mm^{-1}]	2.488	3.632
F (000)	2658.0	3226.0
	$-19 \leq h \leq 26$	$-25 \leq h \leq 25$
Index ranges	$-27 \leq k \leq 28$	$-25 \leq k \leq 23$
	$-23 \leq l \leq 20$	$-21 \leq l \leq 21$
Reflections collected	31143	28983
Independent refs [Rint]	5539[0.0349]	4092 [0.0409]
date/restraints/parameters	5539/55/268	4092/49/323
Goodness-of-fit on F^2	1.041	1.032
R_1, wR_2 [I>2σ(I)]	0.0712, 0.2322	0.0832, 0.2482
R_1, wR_2 [all data]	0.0820, 0.2434	0.0922, 0.2606

15. Reference

[1] A. Fateeva, P.-A. Chater, C.-P. Ireland, A.-A. Tahir, Y.-Z. Khimyak, P.-V. Wiper, J.-R. Darwent, M.-J. Rosseinsky, *Angew. Chem. Int. Ed.* 2012, **51**, 7440-7444.

[2] T. Ahnfeldt, N. Guillou, D. Gunzelmann, I. Margiolaki, T. Loiseau, G. Ferey, J. Senker, N. Stock, *Angew. Chem. Int. Ed.* 2009, **48**, 5163-5166.

[3] H. Reinsch, M. Feyand, T. Ahnfeldt, N. Stock, *Dalton Trans.* 2012, **41**, 4164-4171.

[4] M. Kruger, A.-K. Inge, H. Reinsch, Y.-H. Li, M. Wahiduzzaman, C.-H. Lin, S.-L. Wang, G. Maurin, N. Stock, *Inorg. Chem.* 2017, **56**, 5851-5862.

[5] T. Loiseau, C. Serre, C. Huguenard, G. Fink, F. Taulelle, M. Henry, T. Bataille, G. Ferey, *Chem. Eur. J.* 2004, **10**, 1373-1382.

[6] H. Embrechts, M. Kriesten, M. Ermer, W. Peukert, M. Hartmann, M. Distaso, *RSC Adv.* 2020, **10**, 7336-7348.

[7] P. Serra-Crespo, E.-V. Ramos-Fernandez, J. Gascon, F. Kapteijn, *Chem. Mater.* 2011, **23**, 2565-2572.

[8] N. Hanikel, X. Pei, S. Chheda, H. Lyu, W. Jeong, J. Sauer, L. Gagliardi, O. M. Yaghi, *Science* 2021, **374**, 454–459

[9] F. Gandara, H. Furukawa, S. Lee, O. M. Yaghi, *J. Am. Chem. Soc.* 2014, **136**, 5271-5274.

[10] S. Lee, E.-A. Kapustin, O. M. Yaghi, *Science* 2016, **353**, 808-811.

[11] E.-D. Bloch, D. Britt, C. Lee, C.-J. Doonan, F.-J. Uribe-Romo, H. Furukawa, J.-R. Long, O. M. Yaghi, *J. Am. Chem. Soc.* 2010, **132**, 14382–14384.

[12] L. Geng, C.-H. Liu, S.-T. Wang, W.-H. Fang, J. Zhang, *Angew. Chem. Int. Ed.* 2020, **59**, 16735-16740.

[13] M. Dan-Hardi, C. Serre, T. Frot, L. Rozes, G. Maurin, C. Sanchez, G. Ferey, *J. Am. Chem. Soc.* 2009, **131**, 10857-10859.

[14] Y.-Y. Sun, D.-F. Lu, Y.-X. Sun, M.-Y. Gao, N. Zheng, C. Gu, F. Wang, J. Zhang, *ACS Mater. Lett.* 2020, **3**, 64-68.

[15] S. Wang, H. Reinsch, N. Heymans, M. Wahiduzzaman, C. Martineau-Corcos, G.-De Weireld, G. Maurin, C. Serre, *Matter* 2020, **2**, 1-11.